© 2017. Published by The Company of Biologists Ltd | Disease Models & Mechanisms (2017) 10, 163-171 doi:10.1242/dmm.027839

RESEARCH ARTICLE

Broad AOX expression in a genetically tractable mouse model does not disturb normal physiology

Marten Szibor[1,2,3,*], Praveen K. Dhandapani[1,2,*], Eric Dufour[2], Kira M. Holmström[1,2], Yuan Zhuang[1], Isabelle Salwig[3], Ilka Wittig[4,5,6], Juliana Heidler[4], Zemfira Gizatullina[7], Timur Gainutdinov[7], German Mouse Clinic Consortium[§], Helmut Fuchs[8], Valérie Gailus-Durner[8], Martin Hrabě de Angelis[8,9,10], Jatin Nandania[11], Vidya Velagapudi[11], Astrid Wietelmann[3], Pierre Rustin[12], Frank N. Gellerich[7,13], Howard T. Jacobs[1,2,‡,¶] and Thomas Braun[3,‡]

ABSTRACT

Plants and many lower organisms, but not mammals, express alternative oxidases (AOXs) that branch the mitochondrial respiratory chain, transferring electrons directly from ubiquinol to oxygen without proton pumping. Thus, they maintain electron flow under conditions when the classical respiratory chain is impaired, limiting excess production of oxygen radicals and supporting redox and metabolic homeostasis. AOX from *Ciona intestinalis* has been used to study and mitigate mitochondrial impairments in mammalian cell lines, *Drosophila* disease models and, most recently, in the mouse, where multiple lentivector-AOX transgenes conferred substantial expression in specific tissues. Here, we describe a genetically tractable mouse model in which *Ciona* AOX has been targeted to the *Rosa26* locus for ubiquitous expression. The *AOX*^{Rosa26} mouse exhibited only subtle phenotypic effects on respiratory complex formation, oxygen consumption or the global metabolome, and showed an essentially normal physiology. AOX conferred robust resistance to inhibitors of the respiratory chain *in organello*; moreover, animals exposed to a systemically applied LD50 dose of cyanide did not succumb. The *AOX*^{Rosa26} mouse is a useful tool to investigate respiratory control mechanisms and to decipher mitochondrial disease aetiology *in vivo*.

KEY WORDS: Mitochondria, Mitochondrial disease, Respiratory chain, Alternative oxidase

[1]Institute of Biotechnology, FI-00014 University of Helsinki, Finland. [2]BioMediTech and Tampere University Hospital, FI-33014 University of Tampere, Finland. [3]Max Planck Institute for Heart and Lung Research, Cardiac Development and Remodelling (Department I), Bad Nauheim D-61231, Germany. [4]Functional Proteomics, SFB 815 Core Unit, Faculty of Medicine, Goethe-University, Frankfurt am Main D-60590, Germany. [5]German Center of Cardiovascular Research (DZHK), Partner site RheinMain, Frankfurt, Germany. [6]Cluster of Excellence "Macromolecular Complexes", Goethe-University, Frankfurt am Main D-60590, Germany. [7]Leibniz Institute for Neurobiology, Magdeburg D-39118, Germany. [8]German Mouse Clinic, Institute of Experimental Genetics, Helmholtz Zentrum München, German Research Center for Environmental Health GmbH, Ingolstaedter Landstrasse 1, Neuherberg 85764, Germany. [9]Chair of Experimental Genetics, Center of Life and Food Sciences Weihenstephan, TU Munich, Emil-Erlenmeyer-Forum 2, Freising-Weihenstephan 85350, Germany. [10]Member of German Center for Diabetes Research (DZD), Ingolstaedter Landstrasse 1, Neuherberg 85764, Germany. [11]Institute for Molecular Medicine Finland, FI-00014 University of Helsinki, Finland. [12]INSERM UMR 1141 and Université Paris 7, Hôpital Robert Debré, Paris 75019, France. [13]Department of Neurology, Otto-von-Guericke-University, Magdeburg D-39120, Germany.
*These authors contributed equally to this work.
‡These authors share senior authorship.
§A full list of consortium members appears in Supplementary information

¶Author for correspondence (howard.jacobs@helsinki.fi)

T.G., 0000-0003-1723-1780; H.T.J., 0000-0003-1895-6003

Received 14 September 2016; Accepted 30 November 2016

INTRODUCTION

The mitochondrial system for oxidative phosphorylation (OXPHOS) comprises four multisubunit complexes supporting stepwise respiratory electron flow from primary electron acceptors to oxygen, and a fifth complex (ATP synthase) that uses the proton gradient thereby generated across the inner mitochondrial membrane to synthesize ATP. In many lower organism and plants, alternative oxidases (AOXs) are expressed that branch the mitochondrial respiratory chain, thus transferring electrons directly from ubiquinol to oxygen in a non-proton-motive manner. AOXs are absent in mammals (Young et al., 2013) (Fig. 1A). Their main physiological role is to maintain electron flow under conditions when the classical respiratory chain is impaired, limiting excess production of oxygen radicals and supporting redox and metabolic homeostasis. Because AOX is also found in some invertebrate phyla (McDonald et al., 2009), we have proposed that its expression in commonly studied animal models could be used to elucidate the pathophysiology underlying mitochondrial OXPHOS disorders, providing a rational basis for its eventual implementation in therapeutic applications (Rustin and Jacobs, 2009; El-Khoury et al., 2014).

In earlier studies, AOX from the tunicate *Ciona intestinalis*, a sister group to the vertebrates, was shown to be expressible and catalytically active in human cells (Hakkaart et al., 2006). It was found to alleviate the deleterious consequences of toxic or pathological inhibition of the downstream portion of the mitochondrial respiratory chain (Hakkaart et al., 2006; Dassa et al., 2009), specifically OXPHOS complexes III (cIII) and IV (cIV), which AOX bypasses. A cDNA encoding *Ciona* AOX was subsequently shown to be ubiquitously expressible in *Drosophila*, without eliciting any harmful phenotypic effects (Fernandez-Ayala et al., 2009). In the fly, AOX expression was able to compensate a range of pathological phenotypes at the whole-organism level, including lethality caused by OXPHOS poisons such as antimycin A or cyanide (Fernandez-Ayala et al., 2009), locomotor disturbance or neurodegeneration caused by cIV knockdown (Kemppainen et al., 2014) or other causes of neurodegeneration mimicking Parkinson's (Fernandez-Ayala et al., 2009; Humphrey et al., 2012) or Alzheimer's (El-Khoury et al., 2016) diseases.

The potential for using AOX to study mitochondrial pathophysiology at the whole-organism level in mammals has been demonstrated using lentivector transduction, creating a transgenic mouse expressing *Ciona* AOX in multiple tissues (El-Khoury et al., 2013). Notably, harmful phenotypes were again not seen, despite widespread transgene expression. However, the methodological issues arising from the nature of that model have precluded its widespread use. On insertion of AOX transgenes at multiple genomic sites in the model, none of them individually conferred expression at a high level or in all tissues. Thus, the model could not be combined

Disease Models & Mechanisms (2017) 10, 163-171 doi:10.1242/dmm.027839

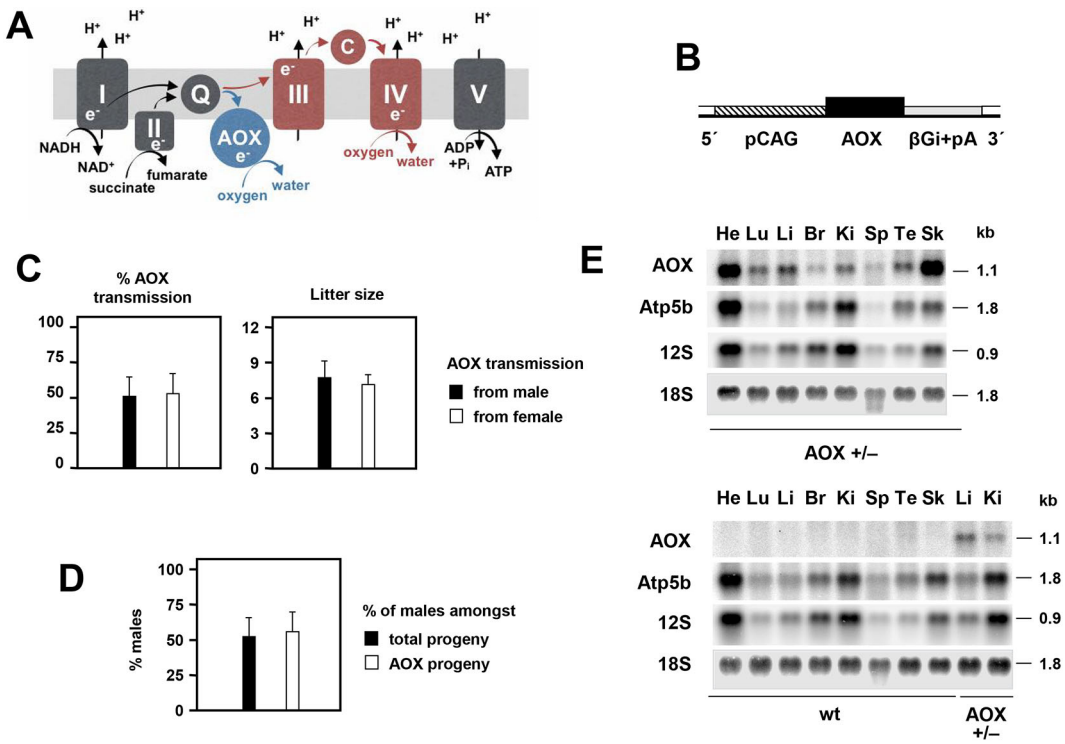

Fig. 1. Construction and characterization of *AOX*^{Rosa26} mice. (A) Schematic diagram of the mitochondrial OXPHOS system, showing the five standard OXPHOS complexes (I-V), the diffusible electron carriers ubiquinone (Q) and cytochrome c (c), and the passage of electrons and protons resulting ultimately in the synthesis of ATP from ADP and inorganic phosphate (Pi). The additional presence of AOX, whether supplied transgenically or in organisms naturally endowed with it, provides an alternative route for the reoxidation of ubiquinol by molecular oxygen, without proton pumping. (B) Schematic diagram of inserted Rosa26-AOX expression construct, following removal of additional elements (i.e. DTA negative selectable marker upon targeted integration, and neomycin resistance cassette following FRT-mediated excision *in vivo*). Remaining elements are the CAG promoter, AOX coding sequence and β-globin intron and poly(A) addition signal (βGi+pA). For full details see Fig. S1A. (C) Transmission rate of *AOX* transgenes (based on PCR) and litter sizes, according to sex of *AOX*-hemizygous parent. Transmission rates from male (n=93, 12 crosses) and from female (n=43, 6 crosses) were not significantly different from each other (Student's t-test, P>0.05, mean±s.d.) or from Mendelian expectation of 50% (chi-squared test). Litter sizes produced by *AOX*-hemizygous males and females also showed no significant difference (Student's t-test, P>0.05). (D) Sex (% of males) of transgenic and wild-type progeny of hemizygous *AOX*^{Rosa26} mice (n=136, 18 crosses), again showing no significant differences (Student's t-test, P>0.05, mean±s.d.). (E) Northern blot showing *AOX* expression in RNA (10 μg) from tissues of one-year-old, male, hemizygous *AOX*^{Rosa26} mice and wild-type (wt) littermate controls: He, heart; Lu, lung; Li, liver; Br, brain; Ki, kidney; Sp, spleen; Te, testis; Sk, skeletal muscle. The blot was reprobed for *Atp5b* mRNA as well as mitochondrial 12S and cytosolic 18S rRNAs as loading controls. RNA molecular weights were extrapolated from rRNA migration in the ethidium bromide-stained gel.

with genetic disease models or other mouse mutants, could not be practically transferred into other strain backgrounds, and its long-term maintenance was essentially impossible.

Here, we report the creation of a genetically tractable transgenic mouse that ubiquitously expresses a single copy of *Ciona* AOX at substantial levels, after targeted insertion into the *Rosa26* locus. The *Rosa26* knock-in gave rise to a functional enzyme, which conferred resistance to respiratory poisons. Surprisingly, comprehensive phenotyping revealed only minor, biologically inconsequential effects of AOX expression in the *AOX*^{Rosa26} mouse. The new model offers great promise as a tool for elucidating the mechanisms of mitochondrial pathology and charting the way towards future therapies.

RESULTS

Construction of *AOX*^{Rosa26} mice

To create a genetically tractable mouse model ubiquitously expressing *Ciona* AOX, we used gene targeting into the ubiquitously active *Rosa26* locus (Hitoshi et al., 1991) in mouse embryonic stem cells (ESC) (Soriano, 1999; Srinivas et al., 2001). Previous authors have reported no detectable pathological alterations arising from insertions at this locus (Friedrich and Soriano, 1991; Zambrowicz et al., 1997), and transgene expression seems to be stable (Zambrowicz et al., 1997). To boost expression from the *Rosa26* locus, we incorporated the synthetic CAG enhancer-promoter into the construct (Fig. 1B; Fig. S1), which enhances expression several-fold (Nyabi et al., 2009; Chen et al., 2011). After verification of the insertion in ESCs by Southern blotting (Fig. S1B,C), a chimeric line was established via blastocyst injection, with subsequent elimination of the positive-selectable (neomycin resistance) cassette (Fig. S1A,B) by Flp recombination *in vivo*, following germ-line transmission. Founders were backcrossed over more than seven generations to strain C57Bl/6J, with transgene presence checked at each step by PCR (Fig. S1D). The rate of transmission of the *AOX* transgene from heterozygous parents of either sex did not significantly deviate from 50% (Fig. 1C), nor was there any significant parent-of-origin effect on litter size (Fig. 1C). The progeny sex ratio was also unaffected by the *AOX* transgene (Fig. 1D).

AOX is ubiquitously expressed in the *AOX*^{Rosa26} mouse

Northern blotting (Fig. 1E) confirmed widespread, though somewhat uneven, expression with highest *AOX* mRNA levels in heart and skeletal muscle, but lower expression in brain, taking account of the

Disease Models & Mechanisms (2017) 10, 163-171 doi:10.1242/dmm.027839

loading controls. At the protein level, expression seemed more uniform, but was again highest in heart, skeletal muscle and pancreas, and lowest in brain (Fig. 2A; Fig. S2). Brain expression was highest in newborn mice (Fig. S2C), but declined substantially by one month of age (Fig. S2C). As expected, AOX expression was higher in homozygotes compared with heterozygous animals (Fig. S2D). The enzyme was found to be associated with the membrane fraction of isolated mitochondria after carbonate extraction (Fig. S2E), albeit less tightly bound than some integral membrane proteins of the OXPHOS complexes, such as subunit 1 of cIV (Mtco1).

In each tissue tested, the expression of representative subunits of the five OXPHOS complexes was essentially unaffected by AOX expression (Fig. 2A; Fig. S2A). Moreover, the overall structure of the respiratory membrane, specifically its organization into supercomplexes, was similarly unaltered, based on blue-native electrophoresis (BNE) followed by in-gel histochemistry of heart mitochondria (Fig. 2B), and on BNE combined with western blots for OXPHOS subunits, for eight different tissues (Fig. S2F). In BNE gels, AOX itself migrated mainly at the size of a dimer and as multimers thereof (Fig. S2F,G), rather than associating specifically with any other respiratory complex. In each tissue tested, the mobility of the respiratory chain complexes detected by BNE was identical to that in controls (Fig. S2F). Principal component analysis of metabolite levels in skeletal muscle (Fig. 2C) and heart (Fig. S2H) showed no consistent effect of AOX expression, nor did any of 100 individual metabolites analyzed show any significant difference (Tables S1, S2).

AOX is functional in *AOX*^{Rosa26} mice

We conducted respirometry to determine whether AOX is enzymatically functional in the *AOX*^{Rosa26} knock-in mice. Mitochondria from six tissues (Fig. 3) were tested in a standard protocol for oxygen consumption in the presence of complex I-, II- and IV-linked substrates, successively using inhibitors of cI (rotenone), cIII (antimycin A), AOX (n-propyl gallate) and cIV (cyanide or azide). There were no significant differences when oxygen consumption was compared with that from mitochondria of wild-type littermates, except for substrate oxidation in the presence of antimycin A (i.e. mediated by AOX), which was significant for all tissues tested except brain, where expression was low. Mitochondria from tissues of *AOX*^{Rosa26} mice other than brain showed antimycin A-resistant (AOX-dependent) oxygen consumption between 30% and 70% of the uninhibited level driven by succinate (Fig. 3A), similar also to preliminary measurements in the founder mouse (Fig. S3A). In heart mitochondria from AOX-expressing compared with control mice, antimycin A- and azide-resistant substrate oxidation was evident across a wide range of drug concentrations (Fig. S3B). Compared with littermate controls, mitochondrial ROS production driven by succinate was greatly decreased (Fig. 3B). Interestingly, this was only significant in the absence of rotenone, implicating AOX in providing

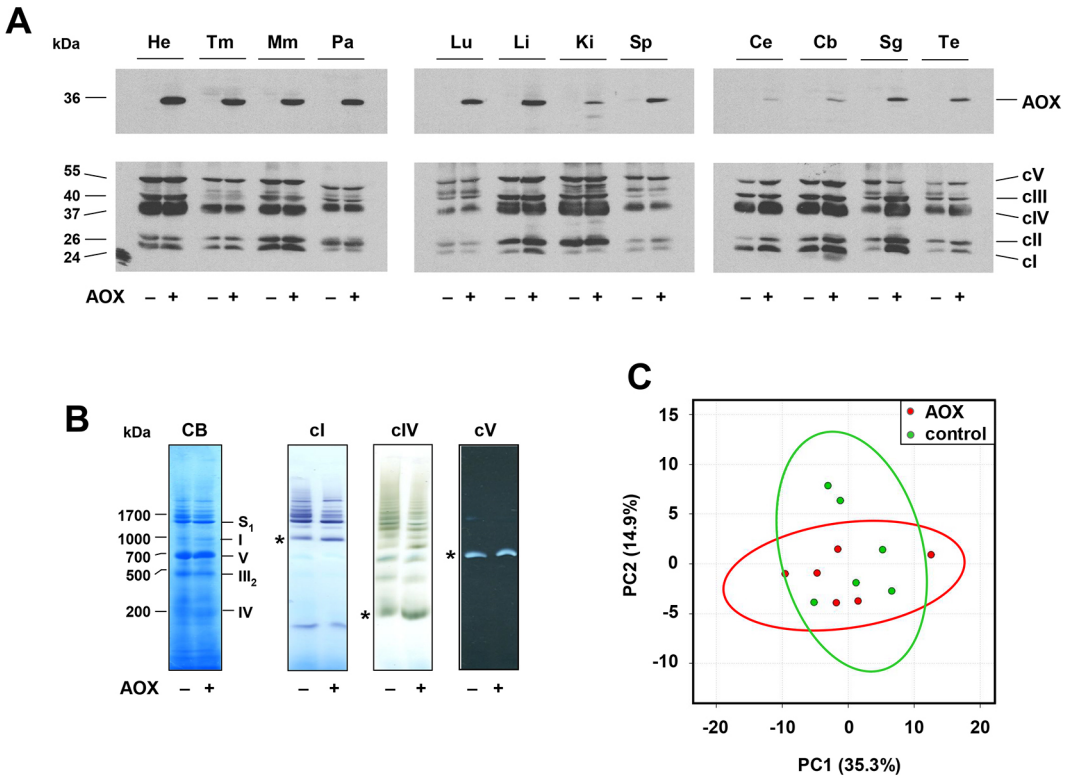

Fig. 2. *AOX*^{Rosa26} mice show broad AOX expression and normal metabolism. (A) Western blots of 20 µg total protein extracts from the indicated tissues (He, heart; Tm, thigh muscle; Mm, masseter muscle; Pa, pancreas; Lu, lung; Li, liver; Ki, kidney; Sp, spleen; Ce, cerebrum; Cb, cerebellum; Sg, salivary gland; Te, testis) of 54-week-old male hemizygous *AOX*^{Rosa26} (+) and wild-type littermate control (–) mice, probed for AOX and for representative subunits of the five OXPHOS complexes (see Materials and Methods, protein molecular weights extrapolated from markers). For Ponceau S staining of the membranes see Fig. S2B. See also Fig. S2A,C,D. (B) BNE gels of mitochondrial membrane proteins from hemizygous *AOX*^{Rosa26} (+) and wild-type littermate control (–) mice, stained with Coomassie Blue (CB) or probed by in-gel histochemistry for the indicated OXPHOS complexes. * denotes the migration of the respective monomeric complexes. Assignment of mitochondrial complexes (I, cI; III_2, dimeric cIII; IV, cIV; V, cV; S_1, respiratory supercomplexes containing cI, dimeric cIII and one copy of cIV) is based on protein molecular weights extrapolated from the migration of the complexes from bovine heart mitochondria, whose subunit composition is known. (C) Principal component analysis of metabolome data from skeletal muscle of hemizygous *AOX*^{Rosa26} (red circles) and wild-type littermate control mice (green circles). The two sets of analysed data overlap, apart from two minor outliers from the control group. See also Fig. S2H.

Disease Models & Mechanisms (2017) 10, 163-171 doi:10.1242/dmm.027839

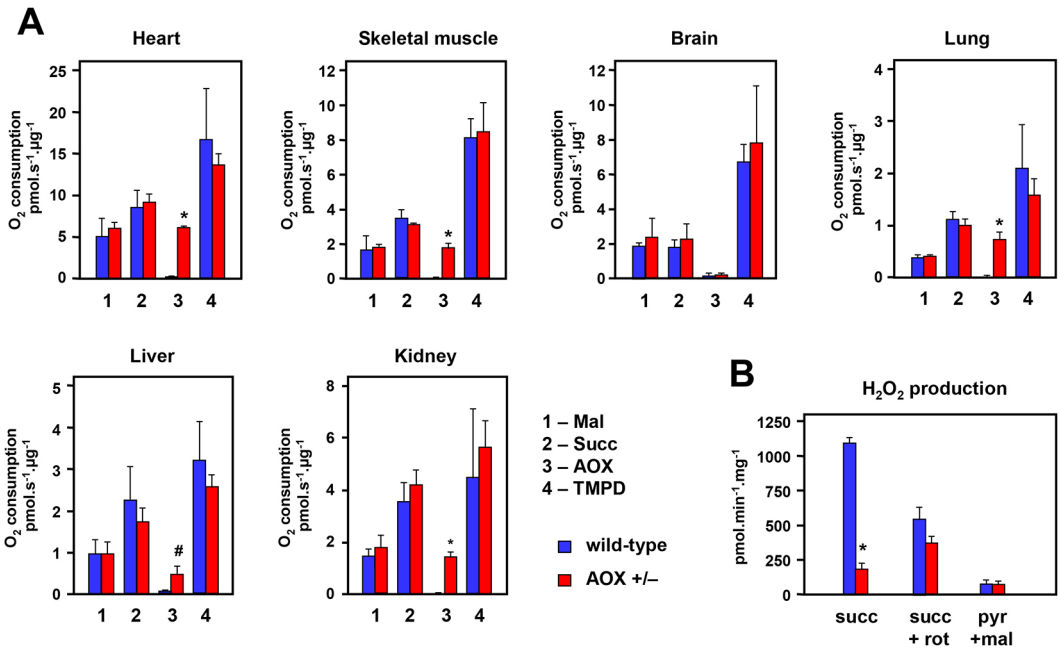

Fig. 3. AOX is enzymatically functional in mitochondria from *AOX*^{Rosa26} mice. (A) Respirometry (oxygen consumption in the indicated units) from isolated mitochondria prepared from the indicated tissues of hemizygous *AOX*^{Rosa26} mice and wild-type littermate controls, as shown; means±s.d. of three biological replicates in each case. Note the different scales. 1 (Mal) – rotenone-sensitive oxidation of malate in the presence of glutamate, pyruvate and ADP; 2 (Succ) – antimycin A- plus n-propyl gallate-sensitive succinate oxidation; 3 (AOX) – rate of n-propyl gallate-sensitive, antimycin A-insensitive succinate oxidation; 4 (TMPD) – rate of ascorbate-reduced TMPD oxidation. For further details see Materials and Methods. See Fig. S3C for respiratory control ratio in these samples. (B) ROS production, measured as H_2O_2 output, from heart mitochondria of *AOX*^{Rosa26} mice and wild-type littermates, as indicated, driven by the indicated substrates or inhibitors (succ, succinate; rot, rotenone; pyr, pyruvate; mal, malate). $^{\#}P<0.05$ or $^{*}P<0.001$ between given pairs of control and *AOX*^{Rosa26} values, Student's *t*-test, means±s.d. Note that it is not possible to verify that this effect depends on the enzymatic activity of AOX, because the AOX inhibitor, n-propyl gallate, is itself a potent antioxidant.

an alternative pathway for succinate oxidation other than reverse electron transport through cI.

AOX^{Rosa26} mice exhibit normal physiology

The high level of AOX expression, capable of replacing a large fraction of electron flow when cIII/IV is inhibited, raised the question of potentially deleterious consequences under normal physiological conditions. Surprisingly, *AOX*^{Rosa26} mice of both sexes were similar in size to littermate controls and gained weight normally during development (Fig. 4A). Muscle and heart functions showed no significant differences from littermate controls, based on standard assays of grip strength (Fig. 4B), treadmill performance (Fig. 4B), cardiac ejection fraction (Fig. 4C) and left ventricular mass (LVM; Fig. 4C), conducted on mice of different ages. To complement these data we implemented a comprehensive phenotyping, using the resources of the German Mouse Clinic (https://www.mouseclinic.de, search 'phenomap'; hereafter referred to as 'GMC Phenomap'). This analysis covered metabolic, behavioural, morphological, immunological, cardiac and neurological parameters, amongst others. None of the parameters tested showed substantial or systematic deviations from littermate controls.

AOX confers protection against an LD50 dose of systemically delivered cyanide

Despite the absence of any meaningful phenotype under standard (non-stressful) physiological conditions, we reasoned that the ubiquitous expression (Fig. 2) of functional AOX (Fig. 3) should confer whole-organism resistance to a respiratory poison targeting cIII or cIV. Sample cohorts of female mice were thus tested for their response to systemically administered potassium cyanide at ∼LD50 (Yamamoto, 1995), with evaluation of survival after 1, 24 and 48 h. All five *AOX*^{Rosa26} transgenic mice tested survived the treatment, whereas three of six littermate controls succumbed as expected (Fig. 5). Although the sample sizes are small, hence indicative rather than definitive, the result is consistent with protection against cyanide at the whole-organism level.

DISCUSSION

In this study we successfully engineered mice for stable, ubiquitous expression of *Ciona* AOX, via a single-copy insertion into the *Rosa26* locus, controlled by the synthetic CAG promoter. AOX protein was widely expressed and enzymatically functional when tested in the presence of antimycin A *in organello*. AOX expression produced negligible phenotypic effects under standard physiological conditions, but seemed able to protect mice from the lethal effects of injected cyanide. The *AOX*^{Rosa26} mouse provides a genetically tractable tool for analyzing the pathophysiology of a wide spectrum of diseases proposed to be linked to mitochondrial respiratory dysfunction.

The *AOX*^{Rosa26} mouse is a genetically tractable model

The 'MitAOX' transgenic mice, previously generated by lentivector transduction (El-Khoury et al., 2013), provided a preliminary indication that widespread *Ciona* AOX expression in the mouse is not harmful. However, owing to the multi-copy nature of the inserted transgene at different genomic sites, as well as varying expression levels, MitAOX mice were not suitable for studies using genetic disease models. To avoid these problems, we created a revised model containing a single insertion of *AOX* cDNA at the *Rosa26* locus on chromosome 6. We demonstrated (Fig. 1) that the

Disease Models & Mechanisms (2017) 10, 163-171 doi:10.1242/dmm.027839

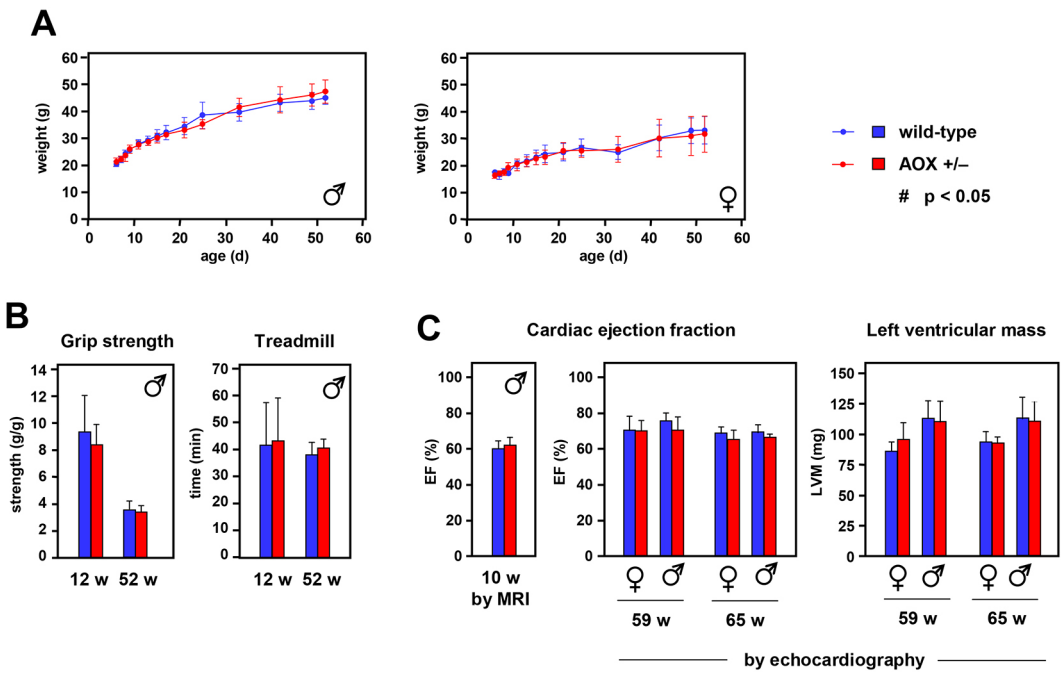

Fig. 4. *AOX*^{Rosa26} mice exhibit normal physiology. (A) Mean weight±s.d. of hemizygous *AOX*^{Rosa26} and wild-type littermate control mice of the sexes indicated, during post-natal development, $n \geq 8$ for each sex and genotype analysed. (B) Muscle parameters of male hemizygous *AOX*^{Rosa26} and wild-type littermate control mice of the ages indicated; means±s.d. For each group analysed $n \geq 4$ (grip strength) or $n \geq 6$ (treadmill). (C) Cardiac parameters, as indicated, of hemizygous *AOX*^{Rosa26} and wild-type littermate control mice of the sex and ages indicated; means±s.d., $n \geq 4$ for each group analysed. All data obtained by echocardiography except ejection fraction at 10 w of age, which used MRI, $n \geq 5$. There were no significant differences between *AOX*^{Rosa26} and wild-type values for any parameter measured (Student's *t*-test, $P > 0.05$).

introduced AOX gene is stably transmitted in a Mendelian manner, remains active beyond at least seven generations of backcrossing to strain C57Bl/6J, shows no parent-of-origin or sex-specific lethality, and is widely expressed. The AOX transgene can, in principle, be transferred to any desired strain background suitable for combination with a given genetic model of disease, although our current analysis was confined to the C57Bl/6J genetic background. We expect that the *AOX*^{Rosa26} mouse will become a versatile model for studying the nature of mitochondrial involvement in disease-like phenotypes.

AOX seems inert under standard physiological conditions

Although AOX was enzymatically functional in the presence of antimycin A *in organello*, our data indicate that the metazoan enzyme is functionally inert under standard physiological conditions, as suggested previously (Hakkaart et al., 2006; Fernandez-Ayala et al., 2009; El-Khoury et al., 2013). Several lines of evidence support this conclusion: (1) any substantial contribution by the non-proton-motive AOX to respiratory electron flow should manifest in a significantly decreased respiratory control ratio in respirometric measurements *in organello*. However, we did not observe any significant alteration in our tissue survey at least for cI-linked substrates and within the detection limits of the method applied (Fig. S3C). (2) Inefficient mobilization of nutritional resources by AOX-expressing mice should alter metabolic parameters *in vivo*. However, there were no differences in whole body weight (Fig. 4A), fat or lean body mass determined by nuclear magnetic resonance (NMR) (see GMC Phenomap), or physiological parameters determined by indirect calorimetry, including food intake, body temperature, oxygen/CO_2 exchange or activity (see GMC Phenomap). (3) No significant differences in heart performance were detected by electro- or echocardiography, or MRI (Fig. 4C; GMC Phenomap), although the heart is the most energy-demanding tissue and showed the highest AOX expression.

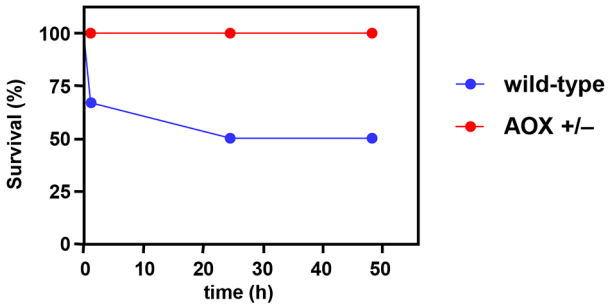

Fig. 5. Sampled *AOX*^{Rosa26} mice are protected against cyanide toxicity *in vivo*. Survival curves of samples of hemizygous female *AOX*^{Rosa26} mice (n=5) and wild-type controls (n=6) treated systemically with KCN as described in Materials and Methods. Note that the experiment would need to be conducted on a much greater scale to generate fully reliable statistics, but is precluded by ethical considerations.

Low AOX expression in brain

The relatively low expression of the *AOX* transgene in adult brain (Fig. 1E, Fig. 2A, Fig. S2A,D) is somewhat puzzling, given previous reports. The CAG promoter has previously been used to drive transgene expression at a high level in the mouse brain during development (Liu et al., 2014) as well as in the adult (Ida-Hosonuma et al., 2002; Kim et al., 2013), and the *Rosa26* locus efficiently drives expression in the brain (Banares et al., 2005; Hitz et al., 2007; Delaunay et al., 2009). Moreover, we also achieved substantial expression in the brains of MitAOX transgenic mice (El-Khoury et al., 2013), using the same CAG promoter.

Disease Models & Mechanisms (2017) 10, 163-171 doi:10.1242/dmm.027839

Intriguingly, neonatal AOX^{Rosa26} brains expressed substantially more AOX at the protein level than adults (Fig. S2C), indicating that the transgene can be active, but apparently regulated, in neural cells. At present we do not have a convincing explanation for these anomalies. However, the relatively low expression of AOX in the adult brain seemed sufficient to protect against the lethality of systemically delivered cyanide (Fig. 5), which can cross the blood-brain barrier and has major toxic effects in the central nervous system (Yamamoto and Tang, 1996; Reiter et al., 2010; Zhang et al., 2015). It will be interesting to explore in greater depth the specific physiological effects of this dose of cyanide and how these effects are modified by AOX expression.

Lack of metabolic disturbance resulting from AOX expression

The lack of any discernible, deleterious phenotype at the whole-organism level arising from AOX expression (Fig. 4; supplementary Data), mirrors the lack of biochemical disturbance in the AOX^{Rosa26} mouse. This was the case even in heart (Fig. 2A,B) and skeletal muscle (Fig. 2A) tissues showing high levels of AOX expression. The highly proteinaceous inner mitochondrial membrane is organized into different subcompartments with distinct structures, protein composition and biochemical functions (Vogel et al., 2006). In particular, the supramolecular organization of the OXPHOS system in supercomplexes is generally considered to maximize the efficiency of electron flow (Acín-Pérez et al., 2008; Chaban et al., 2014). We observed no structural (Fig. 2B) or functional (Fig. 3A) disturbance of the endogenous respiratory membrane upon AOX expression, which might reflect natural properties of *Ciona* AOX, enabling it to reside in the mitochondria of its parent species. Transgenic AOX seems to form homomeric complexes, rather than associating with (and potentially disrupting) other OXPHOS complexes. The electrophoretic mobility of the standard OXPHOS complexes was indistinguishable from that in controls, in all tissues tested (Fig. 2B; Fig. S2F,G). Our findings imply that these multimers are themselves benign, although it remains unknown whether AOX is structurally arrayed in a similar manner in its natural context in *Ciona*. We reason that, by remaining uncomplexed with other respiratory chain components, the enzyme would be functionally adapted to act as a sink for electrons transferred from diffusible quinols in the inner mitochondrial membrane. Quinone reduction might arise from the operation of diverse dehydrogenases, including, for example, cII, electron transferring flavoprotein dehydrogenase, the mitochondrial isoform of glycerol-3-phosphate dehydrogenase and dihydroorotate dehydrogenase. Under normal physiological conditions, diffusible quinols would be efficiently mopped up by (dimeric) cIII, whether alone or attached to cIV as a supercomplex. As in plants (Hoefnagel and Wiskich, 1998; Castro-Guerrero et al., 2004), AOX would only become active at high quinol concentrations, reflecting its lower affinity for quinols than cIII. Thus, AOX would be brought into play only when quinols accumulate as a result of inhibition or overload of the standard respiratory pathway, as inferred previously in human cells (Dassa et al., 2009). This hypothesis is also consistent with our observation that AOX expression drastically decreases mitochondrial ROS production by heart mitochondria in the presence of high levels of succinate (Fig. 3B), which promotes reverse electron flow through cI (Chouchani et al., 2014). Our observations suggest that AOX might have dramatic consequences under stress, especially in heart and other tissues where it is highly expressed. Tests of this hypothesis will also reveal whether AOX could have beneficial roles in future therapies (El-Khoury et al., 2014). A first demonstration of the utility of AOX^{Rosa26} mice has recently been published (Mills et al., 2016), in which AOX was shown to confer resistance against lethality in models of bacterial sepsis. Further trials, combining AOX^{Rosa26} with specific genetic disease models, should reveal the extent to which AOX can alleviate the pathophysiology of respiratory chain dysfunction. The AOX^{Rosa26} mouse model should have wide applications and is available for the research community, upon request.

MATERIALS AND METHODS

Construction of targeting vector

Standard cloning and recombineering procedures (Liu et al., 2003; Warming et al., 2005) were used to assemble the pRosa26-Aox targeting vector. Briefly, PL451 was adapted to serve as AOX entry vector, by integrating homology arms for the mouse *Rosa26* locus (PL451-Rosa26) upstream and downstream of the neomycin selection cassette. *Ciona* AOX (Hakkaart et al., 2006) was integrated upstream of the selection cassette, and used to co-transform recombineering-competent *Escherichia coli* (EL250) with a *Rosa26*-targeting plasmid (pRosa26-DTA). Positive clones were selected by kanamycin resistance (pRosa26-Aox), verified by PCR and sequencing, and electroporated into v6.5 ESCs following linearization with *Sal*I. After negative (DTA, Diptheria toxin A) and positive (G418) selection, homologous integration was verified by Southern blotting (Koetsier et al., 1993) using gene-specific restriction enzymes and probes to distinguish the wild-type and manipulated alleles (see supplementary Materials and Methods and Fig. S1B,C for further details).

Creation of transgenic mice

ESC clones positive for integration were injected into blastocysts and transferred to pseudopregnant mice. Chimeric males were then backcrossed onto the C57Bl/6J strain background to generate heterozygous animals, and subsequently bred with mice ubiquitously expressing FLP recombinase (Rodríguez et al., 2000), in order to delete the neomycin selection cassette. Mice were backcrossed (>7 generations) to C57Bl/6J females to obtain a clean genetic background for all subsequent studies.

PCR genotyping of AOX^{Rosa26} mice

Crude DNA for genotyping was extracted from ear punches or tail cuts by standard methods (proteinase K treatment, isopropanol precipitation and overnight resuspension in TE at 56°C). Multiplex PCR genotyping was carried out using primers Aox 317 s: 5′-GCGATGCAAGATGGAGGGTA-3′ plus Aox 317 as: 5′-TGAATCCAACCGTGGTCTCG-3′ for *AOX*, and Rosa26_wt s: 5′-GACCTCCATCGCGCACTCCG-3′ plus Rosa26_wt as: 5′-CTCCGAGGCGGATCACAAGC-3′ for the wild-type *Rosa26* locus, giving respective products of 317 and 523 bp. PCR reactions of 20 µl contained 4 pmol of each primer, DMSO at 2% and 0.2 µl DyNazyme II (Thermo Fisher Scientific), with cycle parameters of initial denaturation at 95°C for 5 min, then 39 cycles of denaturation at 95°C for 20 s, annealing at 56°C for 30 s and extension at 72°C for 60 s, with final extension step at 72°C for 10 min, followed by 1.5% agarose gel electrophoresis. See Fig. S1D for example gel.

RNA analysis

RNA was prepared from dissected mouse tissues by bead homogenization in 700 µl (>10 volumes) of Trizol reagent (Sigma). After incubation for 5 min at room temperature, samples were gently extracted with 0.2 volumes of chloroform and centrifuged at 12,000 $\boldsymbol{g}_{max}$ for 15 min at 4°C. The upper (aqueous) phase was decanted and RNA recovered by isopropanol precipitation and centrifugation. Using standard procedures (Sambrook et al., 1989), air-dried RNA pellets were resuspended in 20 µl RNase-free water, fractionated on formaldehyde-agarose gels, blotted to Hybond-N+ membrane (GE Healthcare) in 10×SSC and hybridized to end-labelled DNA oligonucleotide probes for *AOX*, mitochondrial 12S and cytosolic 18S rRNA, and *Atp5b* mRNA, respectively 5′-CTTGACCCACTGTTTCTCA-TCTAGCCG-3′, 5′-CATGGGCTACACCTTGACCT-3′, 5′-TCGAACCC-TGATTCCCCGTCACCC-3′ and 5′-GGTGAATATGACCATCTCCCAG-AACAAGC-3′.

Disease Models & Mechanisms (2017) 10, 163-171 doi:10.1242/dmm.027839

Protein analysis

For protein extraction, small pieces of fresh or frozen tissue from dissected organs were placed in 500 µl of lysis buffer (50 mM Tris/HCl, 150 mM NaCl, 1 mM EDTA, 1% Triton X-100, pH 7.4), containing a dissolved protease inhibitor cocktail tablet (Pierce), in a 5 ml tube on ice. After homogenization using a POLYTRON PT 1200 E Manual Disperser (Ecoline), samples were incubated on ice for 30 min followed by centrifugation at 14,000 g_{max} for 5 min at 4°C. Supernatants were saved and protein concentration was measured using Bradford reagent (Bio-Rad) before dilution into SDS-PAGE sample buffer for electrophoresis on SDS 12% polyacrylamide gels. After semi-dry transfer to PROTRAN nitrocellulose membranes (PerkinElmer), western blots were probed using primary antibodies for AOX [customized rabbit antibody, 21st Century Biochemicals (Fernandez-Ayala et al., 2009), 1:40,000 in Tris-buffered saline (TBST) containing 5% BSA] with secondary antibody peroxidase-conjugated AffiniPure goat anti-rabbit IgG (Jackson ImmunoResearch, 111-035-144, 1:20,000). After stripping by two 20 min washes with 100 mM β-mercaptoethanol, 2% SDS, 62.5 mM Tris-HCl (pH 6.7), each followed by blocking with TBST containing 5% milk for 30 min, blots were reprobed for representative subunits of the OXPHOS complexes, using Total OXPHOS Cocktail antibody [Abcam, ab110413, 1:250; visualizing Sdhb (cII), Uqcrc2 (cIII), Mtco1 (cIV) and Atp5a (cV)], plus an antibody against complex 1 subunit Ndufs3 (Mitosciences, ab14711, 1:4000), both detected with peroxidase-conjugated AffiniPure goat anti-mouse IgG (Jackson ImmunoResearch, 115-035-146, 1:1000) as secondary antibody. Chemiluminescent detection used 20× LumiGLO Reagent and 20× Peroxide from Cell Signaling Technology, according to manufacturer's recommendations. Enrichment of mitochondrial membranes, solubilisation of mitochondrial complexes and BNE were carried out as described (Wittig et al., 2006; Heidler et al., 2013). Mitochondrial complexes were stained with Coomassie Blue (Wittig et al., 2006) and specific in-gel histochemical staining for cI, cIV, and cV was performed as described previously (Wittig et al., 2007). For immunodetection, BNE-gels were blotted onto PVDF membranes and probed with antibodies against AOX (1:50,000) or mitochondrial complexes (MitoProfile Total OXPHOS Rodent WB Antibody Cocktail, Mitosciences, ab110413, 1:250) and cIV (1:1000; Heidler et al., 2013).

Metabolomics

Metabolite analysis was conducted as described previously (Nikkanen et al., 2016), using skeletal muscle from six hemizygous AOX^{Rosa26} and six wild-type littermate control mice (8-week-old males, all culled at a single time in the morning). Briefly, targeted metabolomics was implemented by ultra-performance liquid chromatography tandem mass-spectrometry using a Waters XEVO-TQ-S mass spectrometer. Metabolites extracted with acetonitrile were separated by hydrophilic liquid-interaction chromatography, then analysed spectrometrically by multiple reaction monitoring. Raw data were collected and analysed with TargetLynx software (Waters), and metabolites quantified using internal standards and calibration curves. For full details, see supplementary Materials and Methods.

Bioenergetic experiments

For respirometry of mitochondria from different tissues, mice were euthanised by cervical dislocation and organs were dissected and collected into ice-cold PBS. Soft tissues were fine chopped (1 mm^3) in ice-cold PBS and hand-homogenized in 3 ml re-suspension buffer [225 mM sucrose, 75 mM D-mannitol, 10 mM Tris/HCl, 1 mM EGTA, 1 mg/ml bovine serum albumin (BSA), pH 7.4], using a glass-teflon homogenizer (tight-fitting pestle). Hard tissues (heart, skeletal muscle and kidney), chopped to a similar size, were pre-treated with 3 ml (~10 volumes) ice-cold trypsin-EDTA [500 µg/ml trypsin (Difco), 0.5 mM EDTA, 10 µg/ml phenol red, pH 7.4] for 10 min, followed by blocking with 300 µl foetal bovine serum (Gibco/Life Technologies) and recovery by low-speed centrifugation (40 g_{max}, 1 min, 4°C) before homogenization. Homogenates were centrifuged at 1300 g_{max} for 5 min at 4°C, after which supernatants were collected and re-centrifuged at 17,000 g_{max} for 15 min at 4°C. The mitochondrial pellet was resuspended, according to its size, in 75-250 µl ice-cold MiR05 buffer [0.5 mM EGTA, 3 mM $MgCl_2$, 60 mM lactobionic acid (Aldrich, buffered to pH 7.0 with 5 M KOH), 20 mM taurine (Sigma), 10 mM KH_2PO_4, 20 mM HEPES/KOH, 110 mM sucrose and 1 g/l fatty-acid free BSA (Sigma), pH 7.2 at room temperature] and stored on ice until respirometry. Mitochondrial protein content was assayed using Bradford reagent (Bio-Rad). Respirometry, using an O2K oxygraph (Oroboros), was conducted in MiR05 buffer in a 2 ml chamber, to which was added 50 or 100 µg of mitochondria according to the tissue. Substrates and inhibitors were added in the following order: (1) 5 mM sodium pyruvate+5 mM sodium glutamate+5 mM sodium malate, (2) 4 mM ADP, (3) 150 nM rotenone (Sigma), (4) 17 mM sodium succinate, (5) 22.5 ng/ml antimycin A (Sigma), (6) 200 µM n-propyl gallate (nPG, Sigma), (7) 0.5 mM N,N,N′,N′-tetramethyl-p-phenylenediamine (TMPD, Sigma) +2 mM sodium L-ascorbate, (8) 100 mM NaN_3 or 1 mM KCN. The flux values [pmol/(s×ml)] obtained from the trace were normalized to the amount of mitochondrial protein. For measurements of ROS production, mouse heart mitochondria were isolated essentially as described (Mela and Seitz, 1979), with minor modifications: tissue was minced in 225 mM mannitol, 20 mM MOPS, 75 mM sucrose, 1 mM EGTA, 0.5 mM dithiothretol, pH 7.4 and hand-homogenized in 10 ml/g tissue of the same buffer containing 0.05% Nagarse (Sigma). After addition of 30 ml of the original buffer, the homogenate was centrifuged at 2000 g_{max} for 4 min at 4°C. The supernatant was passed through cheesecloth and re-centrifuged at 12,000 g_{max} for 10 min. The resulting pellet was resuspended in 225 mM mannitol, 20 mM MOPS, 75 mM sucrose, 0.1 mM EGTA, 75 mM KCl, pH 7.4. Mitochondrial protein content was determined using the bicinchoninic acid assay (Wiechelman et al., 1988), with BSA as standard. ROS production under conditions used for respirometry was measured fluorimetrically using 5 µM Amplex Red (Hydrogen Peroxide Assay Kit, Thermo Fisher Scientific) and 3 units/ml horseradish peroxidase at 30°C, using a Carry Eclipse fluorimeter (Varian) with excitation at 560 nm and detection at 590 nm (Zhou et al., 1997).

Mouse phenotyping

Mouse body weight was measured using a small electronic balance suitable for rodents. Grip strength was measured using the BIO-GS3 apparatus (Bioseb). Mice were placed on the platform until all four limbs were engaged on the grid, and then pulled to measure the force generated. The mean of three measurements was normalised to body weight (g/g) for each animal tested. All animals were trained for three successive days before the actual experiment. Endurance running was measured as previously (Yatsuga and Suomalainen, 2012), as the run time on a standard running belt (Exer-6M Treadmill, Columbus Instruments), set to reach a speed of 6.5 m/min in steps of 0.5 m/min every 3 min. A stay of more than 5 s on the electrified motivation grid (0.5 mA current) was considered as the end point of each test. Cardiac parameters (ejection fraction, left ventricular mass) were determined by echocardiography (Vevo 2100 system, FujiFilm VisualSonics Inc.) or, where indicated in figure legends, by magnetic resonance imaging (MRI), performed essentially as described elsewhere (Ziebart et al., 2008). MRI data were analysed using OsiriX Imaging Software (http://www.osirix-viewer.com/index.html). Comprehensive phenotyping by the German Mouse Clinic (GMC) was conducted using the protocols described and referenced at https://www.mouseclinic.de (search 'phenomap'). In all tests, mouse genotypes were blinded to the experimenter and verified subsequently.

Systemic administration of cyanide

The procedure was implemented under contract by Luria Scientific Industries, Herzliya, Israel (responsible scientist Dr Iris Maimon). Mice, whose genotypes were blinded to the experimenter, were anesthetized with 3% isoflurane in an induction chamber, after which anaesthesia was maintained by 2% isoflurane using a nose cone. Core temperature was kept at 36.5°C using a heating pad. KCN was dissolved in distilled water at 10 mg/ml and delivered by IP injection to the mice at 8.5 mg/kg. Animals were observed for 48 h for the onset of death, defined as apnea without further respiratory effort or movement or palpable cardiac pulsation.

Ethical permits

All mouse breeding and experiments were approved by the national ethical committee in Finland, under permits ESAVI/8766/04.10.07/2015 and ESAVI/

2954/04.10.07/2015. Mouse experiments conducted under contract by Luria Scientific Industries were approved by IACUC under assurance 7433J45, 07/22/2015. Maintenance of mice in Magdeburg was in accord with procedures specified by the Animal Health and Care Committees of the Otto-von-Guericke University, Magdeburg, and of the State of Sachsen-Anhalt, Germany.

Image processing

Images were optimized for brightness and contrast and cropped for clarity. No other manipulations such as gamma corrections were made, nor was any relevant information excluded by cropping. Full, original gel images are available on request.

Acknowledgements

We thank Maarit Myöhänen, Sonja Krüger, Susanne Kreutzer, Birgit Spitznagel and Jana Meisterknecht for excellent technical assistance, Christopher Carroll, Giuseppe Cannino, Luca Giordano, Riikka Kivelä and Uwe Richter for technical advice and help, Anu Suomalainen and Brendan Battersby, for useful discussions, and Troy Faithfull for critical reading of the manuscript.

Competing interests

The authors declare no competing or financial interests.

Author contributions

H.T.J., T.B., P.R. and M.S. jointly conceived the project and developed the strategy to create the *AOX*^{Rosa26} mouse. M.S. supervised and coordinated the laboratory work, which was conducted by M.S., P.K.D., E.D., K.M.H., Y.Z., I.S., I.W., J.H., Z.G., T.G., J.N., V.V., A.W. and F.N.G. H.F., V.G.-D. and M.H.d.A. implemented comprehensive phenotyping in collaboration with their colleagues from the German Mouse Clinic. H.T.J. compiled the manuscript and figures with assistance from all authors.

Funding

This work was supported by funding from the European Research Council (Advanced Grant 232738 to H.T.J.), Academy of Finland (Suomen Akatemia) Terveyden Tutkimuksen Toimikunta (grant 272376); Tampere University (Tampereen Yliopisto) Hospital Medical Research Fund; the Sigrid Juselius Foundation (Sigrid Juséliuksen Säätiö), Max-Planck-Gesellschaft, Deutsche Forschungsgemeinschaft (DFG SFB 815 project Z1 to I.W. and DFG SFB 1213 project A2 to T.B.), the Cluster of Excellence “Macromolecular Complexes”, Goethe-Universität Frankfurt am Main, Germany (to I.W.), the Cluster of Excellence “Cardiopulmonary System” (to T.B.), the German Center for Lung Research (DLZ), and the Universities of Helsinki and Tampere (Helsingin Yliopisto and Tampereen Yliopisto). This work has also been funded by the German Federal Ministry of Education and Research (Bundesministerium für Bildung und Forschung) to the German Mouse Clinic (Infrafrontier grant 01KX1012).

Data availability

Comprehensive phenotyping by the German Mouse Clinic (GMC) was conducted using the protocols described and referenced at https://www.mouseclinic.de (search ‘phenomap’).

Supplementary information

Supplementary information available online at
http://dmm.biologists.org/lookup/doi/10.1242/dmm.027839.supplemental

References

Acín-Pérez, R., Fernández-Silva, P., Peleato, M. L., Pérez-Martos, A. and Enriquez, J. A. (2008). Respiratory active mitochondrial supercomplexes. *Mol. Cell* **32**, 529-539.

Banares, S., Zeh, K., Krajewska, M., Kermer, P., Baribault, H., Reed, J. C. and Krajewski, S. (2005). Novel pan-neuronal Cre-transgenic line for conditional ablation of genes in the nervous system. *Genesis* **42**, 6-16.

Castro-Guerrero, N. A., Krab, K. and Moreno-Sánchez, R. (2004). The alternative respiratory pathway of euglena mitochondria. *J. Bioenerg. Biomembr.* **36**, 459-469.

Chaban, Y., Boekema, E. J. and Dudkina, N. V. (2014). Structures of mitochondrial oxidative phosphorylation supercomplexes and mechanisms for their stabilisation. *Biochim. Biophys. Acta* **1837**, 418-426.

Chen, C. M., Krohn, J., Bhattacharya, S. and Davies, B. (2011). A comparison of exogenous promoter activity at the ROSA26 locus using a PhiC31 integrase mediated cassette exchange approach in mouse ESCs. *PLoS ONE* **6**, e23376.

Chouchani, E. T., Pell, V. R., Gaude, E., Aksentijević, D., Sundier, S. Y., Robb, E. L., Logan, A., Nadtochiy, S. M., Ord, E. N. J., Smith, A. C. et al. (2014). Ischaemic accumulation of succinate controls reperfusion injury through mitochondrial ROS. *Nature* **515**, 431-435.

Dassa, E. P., Dufour, E., Gonçalves, S., Paupe, V., Hakkaart, G. A. J., Jacobs, H. T. and Rustin, P. (2009). Expression of the alternative oxidase complements cytochrome c oxidase deficiency in human cells. *EMBO Mol. Med.* **1**, 30-36.

Delaunay, D., Heydon, K., Miguez, A., Schwab, M., Nave, K.-A., Thomas, J. L., Spassky, N., Martinez, S. and Zalc, B. (2009). Genetic tracing of subpopulation neurons in the prethalamus of mice (Mus musculus). *J. Comp. Neurol.* **512**, 74-83.

El-Khoury, R., Dufour, E., Rak, M., Ramanantsoa, N., Grandchamp, N., Csaba, Z., Duvillié, B., Bénit, P., Gallego, J., Gressens, P. et al. (2013). Alternative oxidase expression in the mouse enables bypassing cytochrome c oxidase blockade and limits mitochondrial ROS overproduction. *PLoS Genet.* **9**, e1003182.

El-Khoury, R., Kemppainen, K. K., Dufour, E., Szibor, M., Jacobs, H. T. and Rustin, P. (2014). Engineering the alternative oxidase gene to better understand and counteract mitochondrial defects: state of the art and perspectives. *Br. J. Pharmacol.* **171**, 2243-2249.

El-Khoury, R., Kaulio, E., Lassila, K. A., Crowther, D. C., Jacobs, H. T. and Rustin, P. (2016). Expression of the alternative oxidase mitigates beta-amyloid production and toxicity in model systems. *Free Radic. Biol. Med.* **96**, 57-66.

Fernandez-Ayala, D. J. M., Sanz, A., Vartiainen, S., Kemppainen, K. K., Babusiak, M., Mustalahti, E., Costa, R., Tuomela, T., Zeviani, M., Chung, J. et al. (2009). Expression of the Ciona intestinalis alternative oxidase (AOX) in Drosophila complements defects in mitochondrial oxidative phosphorylation. *Cell Metab.* **9**, 449-460.

Friedrich, G. and Soriano, P. (1991). Promoter traps in embryonic stem cells: a genetic screen to identify and mutate developmental genes in mice. *Genes Dev.* **5**, 1513-1523.

Hakkaart, G. A. J., Dassa, E. P., Jacobs, H. T. and Rustin, P. (2006). Allotopic expression of a mitochondrial alternative oxidase confers cyanide resistance to human cell respiration. *EMBO Rep.* **7**, 341-345.

Heidler, J., Strecker, V., Csintalan, F., Bleier, L. and Wittig, I. (2013). Quantification of protein complexes by blue native electrophoresis. *Methods Mol. Biol.* **1033**, 363-379.

Hitoshi, N., Ken-ichi, Y. and Jun-ichi, M. (1991). Efficient selection for high-expression transfectants with a novel eukaryotic vector. *Gene* **108**, 193-199.

Hitz, C., Wurst, W. and Kühn, R. (2007). Conditional brain-specific knockdown of MAPK using Cre/loxP regulated RNA interference. *Nucleic Acids Res.* **35**, e90.

Hoefnagel, M. H. N. and Wiskich, J. T. (1998). Activation of the plant alternative oxidase by high reduction levels of the Q-pool and pyruvate. *Arch. Biochem. Biophys.* **355**, 262-270.

Humphrey, D. M., Parsons, R. B., Ludlow, Z. N., Riemensperger, T., Esposito, G., Verstreken, P., Jacobs, H. T., Birman, S. and Hirth, F. (2012). Alternative oxidase rescues mitochondria-mediated dopaminergic cell loss in Drosophila. *Hum. Mol. Genet.* **21**, 2698-2712.

Ida-Hosonuma, M., Iwasaki, T., Taya, C., Sato, Y., Li, J., Nagata, N., Yonekawa, H. and Koike, S. (2002). Comparison of neuropathogenicity of poliovirus in two transgenic mouse strains expressing human poliovirus receptor with different distribution patterns. *J. Gen. Virol.* **83**, 1095-1105.

Kemppainen, K. K., Rinne, J., Sriram, A., Lakanmaa, M., Zeb, A., Tuomela, T., Popplestone, A., Singh, S., Sanz, A., Rustin, P. et al. (2014). Expression of alternative oxidase in Drosophila ameliorates diverse phenotypes due to cytochrome oxidase deficiency. *Hum. Mol. Genet.* **23**, 2078-2093.

Kim, H. S., Joo, H. J., Woo, J. S., Choi, Y. S., Choi, S. H., Kim, H. and Moon, W. K. (2013). In vivo magnetic resonance imaging of transgenic mice expressing human ferritin. *Mol. Imaging Biol.* **15**, 48-57.

Koetsier, P. A., Schorr, J. and Doerfler, W. (1993). A rapid optimized protocol for downward alkaline Southern blotting of DNA. *Biotechniques* **15**, 260-262.

Liu, P., Jenkins, N. A. and Copeland, N. G. (2003). A highly efficient recombineering-based method for generating conditional knockout mutations. *Genome Res.* **13**, 476-484.

Liu, Y., Fu, S., Niu, R., Yang, C. and Lin, J. (2014). Transcriptional activity assessment of three different promoters for mouse *in utero* electroporation system. *Plasmid* **74**, 52-58.

McDonald, A. E., Vanlerberghe, G. C. and Staples, J. F. (2009). Alternative oxidase in animals: unique characteristics and taxonomic distribution. *J. Exp. Biol.* **212**, 2627-2634.

Mela, L. and Seitz, S. (1979). Isolation of mitochondria with emphasis on heart mitochondria from small amounts of tissue. *Methods Enzymol.* **55**, 39-46.

Mills, E. L., Kelly, B., Logan, A., Costa, A. S. H., Varma, M., Bryant, C. E., Tourlomousis, P., Däbritz, J. H. M., Gottlieb, E. , Latorre I. et al. (2016). Succinate dehydrogenase supports metabolic repurposing of mitochondria to drive inflammatory macrophages. *Cell* **167**, 457-470.

Nikkanen, J., Forsström, S., Euro, L., Paetau, I., Kohnz, R. A., Wang, L., Chilov, D., Viinamäki, J., Roivainen, A., Marjamäki, P. et al. (2016). Mitochondrial DNA replication defects disturb cellular dNTP pools and remodel one-carbon metabolism. *Cell Metab.* **23**, 635-648.

Nyabi, O., Naessens, M., Haigh, K., Gembarska, A., Goossens, S., Maetens, M., De Clercq, S., Drogat, B., Haenebalcke, L., Bartunkova, S. et al. (2009). Efficient mouse transgenesis using Gateway-compatible ROSA26 locus targeting vectors and F1 hybrid ESCs. *Nucleic Acids Res.* **37**, e55.

Reiter, R. J., Manchester, L. C. and Tan, D. X. (2010). Neurotoxins: free radical mechanisms and melatonin protection. *Curr. Neuropharmacol.* **8**, 194-210.
Rodríguez, C. I., Buchholz, F., Galloway, J., Sequerra, R., Kasper, J., Ayala, R., Stewart, A. F. and Dymecki, S. M. (2000). High-efficiency deleter mice show that FLPe is an alternative to Cre-loxP. *Nat. Genet.* **25**, 139-140.
Rustin, P. and Jacobs, H. T. (2009). Respiratory chain alternative enzymes as tools to better understand and counteract respiratory chain deficiencies in human cells and animals. *Physiol. Plant.* **137**, 362-370.
Sambrook, J., Fritsch, E. F. and Maniatis, T. (1989). *Molecular Cloning: A Laboratory Manual*. New York, USA: Cold Spring Harbor Laboratory Press.
Soriano, P. (1999). Generalized lacZ expression with the ROSA26 Cre reporter strain. *Nat. Genet.* **21**, 70-71.
Srinivas, S., Watanabe, T., Lin, C.-S., William, C. M., Tanabe, Y., Jessell, T. M. and Costantini, F. (2001). Cre reporter strains produced by targeted insertion of EYFP and ECFP into the ROSA26 locus. *BMC Dev. Biol.* **1**, 4.
Vogel, F., Bornhövd, C., Neupert, W. and Reichert, A. S. (2006). Dynamic subcompartmentalization of the mitochondrial inner membrane. *J. Cell. Biol.* **175**, 237-247.
Warming, S., Costantino, N., Court, D. L., Jenkins, N. A. and Copeland, N. G. (2005). Simple and highly efficient BAC recombineering using galK selection. *Nucleic Acids Res.* **33**, e36.
Wiechelman, K. J., Braun, R. D. and Fitzpatrick, J. D. (1988). Investigation of the bicinchoninic acid protein assay: identification of the groups responsible for color formation. *Anal. Biochem.* **175**, 231-237.
Wittig, I., Braun, H.-P. and Schägger, H. (2006). Blue native PAGE. *Nat. Protoc.* **1**, 418-428.
Wittig, I., Karas, M. and Schägger, H. (2007). High resolution clear native electrophoresis for in-gel functional assays and fluorescence studies of membrane protein complexes. *Mol. Cell. Proteomics* **6**, 1215-1225.
Yamamoto, H. (1995). Effect of atropine on cyanide-induced acute lethality in mice. *Toxicol. Lett.* **80**, 29-33.
Yamamoto, H. and Tang, H. W. (1996). Antagonistic effect of melatonin against cyanide-induced seizures and acute lethality in mice. *Toxicol Lett.* **87**, 19-24.
Yatsuga, S. and Suomalainen, A. (2012). Effect of bezafibrate treatment on late-onset mitochondrial myopathy in mice. *Hum. Mol. Genet.* **21**, 526-535.
Young, L., Shiba, T., Harada, S., Kita, K., Albury, M. S. and Moore, A. L. (2013). The alternative oxidases: simple oxidoreductase proteins with complex functions. *Biochem. Soc. Trans.* **41**, 1305-1311.
Zambrowicz, B. P., Imamoto, A., Fiering, S., Herzenberg, L. A., Kerr, W. G. and Soriano, P. (1997). Disruption of overlapping transcripts in the ROSA beta geo 26 gene trap strain leads to widespread expression of beta-galactosidase in mouse embryos and hematopoietic cells. *Proc. Natl. Acad. Sci. USA* **94**, 3789-3794.
Zhang, D., Lee, B., Nutter, A., Song, P., Dolatabadi, N., Parker, J., Sanz-Blasco, S., Newmeyer, T., Ambasudhan, R., McKercher, S. R. et al. (2015). Protection from cyanide-induced brain injury by the Nrf2 transcriptional activator carnosic acid. *J. Neurochem.* **133**, 898-908.
Zhou, M., Diwu, Z., Panchuk-Voloshina, N. and Haugland, R. P. (1997). A stable nonfluorescent derivative of resorufin for the fluorometric determination of trace hydrogen peroxide: applications in detecting the activity of phagocyte NADPH oxidase and other oxidases. *Anal. Biochem.* **253**, 162-168.
Ziebart, T., Yoon, C.-H., Trepels, T., Wietelmann, A., Braun, T., Kiessling, F., Stein, S., Grez, M., Ihling, C., Muhly-Reinholz, M.et al. (2008). Sustained persistence of transplanted proangiogenic cells contributes to neovascularization and cardiac function after ischemia. *Circ. Res.* **103**, 1327-1334.

DETAILS OF GERMAN MOUSE CLINIC CONSORTIUM MEMBERS

Antonio Aguilar-Pimentel[1]
Markus Ollert[3]
Carsten Schmidt-Weber[10]
Lore Becker[1,4]
Thomas Klopstock[4,14,15,18,19]
Thure Adler[1]
Irina Treise[1]
Dirk H. Busch[2]
Marion Horsch[1]
Johannes Beckers[1,16,17]
Kristin Moreth[1]
Raffi Bekeredjian[5]
Lillian Garrett[1,7]
Sabine M. Hölter[1,7]
Annemarie Zimprich[1,7]
Wolfgang Wurst[7,13,14,15]
Wolfgang Hans[1]
Oana Amarie[1,7]
Jochen Graw[7]
Jan Rozman[1,17]
Martin Klingenspor[8,9]
Julia Calzada-Wack[1,6]
Patricia da Silva-Buttkus[1,6]
Frauke Neff[1,6]
Ildiko Racz[1,11]
Andreas Zimmer[11]
Birgit Rathkolb[1,12,17]
Eckhard Wolf[12]
Manuela Östereicher[1]
Ralph Steinkamp[1]
Christoph Lengger[1]
Holger Maier[1]

Claudia Stoeger[1]
Stefanie Leuchtenberger[1]
Valérie Gailus-Durner[1]
Helmut Fuchs[1]
Martin Hrabě de Angelis[1,16,17]

[1]German Mouse Clinic, Institute of Experimental Genetics, Helmholtz Zentrum München, German Research Center for Environmental Health GmbH, Ingolstädter Landstrasse 1, 85764 Neuherberg, Germany
[2]Institute for Medical Microbiology, Immunology and Hygiene, Technical University of Munich, Trogerstrasse 9, 81675 Munich, Germany
[3]Department of Infection and Immunity, Luxembourg Institute of Health, Esch-sur-Alzette, Luxembourg, and Department of Dermatology and Allergy Center, Odense Research Center for Anaphylaxis, University of Southern Denmark, Odense, Denmark
[4]Department of Neurology, Friedrich-Baur-Institut, Ludwig-Maximilians-Universität München, Ziemssenstrasse 1a, 80336 Munich, Germany
[5]Department of Cardiology, University of Heidelberg, Im Neuenheimer Feld 410, 69120 Heidelberg, Germany
[6]Institute of Pathology, Helmholtz Zentrum München, German Research Center for Environmental Health GmbH, Ingolstädter Landstrasse 1, 85764 Neuherberg, Germany
[7]Institute of Developmental Genetics, Helmholtz Zentrum München, German Research Center for Environmental Health GmbH, Ingolstädter Landstrasse 1, 85764 Neuherberg, Germany
[8]Chair for Molecular Nutritional Medicine, Technische Universität München, Else Kröner-Fresenius Center for Nutritional Medicine, 85350 Freising, Germany
[9]ZIEL – Center for Nutrition and Food Sciences, Technische Universität München, 85350 Freising, Germany
[10]Center of Allergy & Environment (ZAUM), Technische Universität München and Helmholtz Zentrum, Biedersteiner Str. 29, 80802 Munich, Germany, and Member of the German Center for Lung Research (DZL), Aulweg 130, 35392 Gießen, Germany
[11]Institute of Molecular Psychiatry, Medical Faculty, University of Bonn, Sigmund-Freud-Strasse 25, 53127 Bonn, Germany

[12]Ludwig-Maximilians-Universität München, Gene Center, Institute of Molecular Animal Breeding and Biotechnology, Feodor-Lynen Strasse 25, 81377 Munich, Germany

[13]Chair of Developmental Genetics, Center of Life and Food Sciences Weihenstephan, Technische Universität München, Ingolstädter Landstrasse 1, 85764 Neuherberg, Germany

[14]Deutsches Institut für Neurodegenerative Erkrankungen (DZNE) Site Munich, Schillerstrasse 44, 80336 Munich, Germany

[15]Munich Cluster for Systems Neurology (SyNergy), Adolf-Butenandt-Institut, Ludwig-Maximilians-Universität München, Schillerstrasse 44, 80336 Munich, Germany

[16]Chair of Experimental Genetics, Center of Life and Food Sciences Weihenstephan, TU Munich, Emil-Erlenmeyer-Forum 2 , 85350 Freising-Weihenstephan, Germany

[17]Member of German Center for Diabetes Research (DZD), Ingolstädter Landstraße 1, 85764 Neuherberg, Germany

[18]German Network for Mitochondrial Disorders (mitoNET)

[19]German Center for Vertigo and Balance Disorders, Munich, Germany

SUPPLEMENTARY MATERIALS AND METHODS

Construction of targeting vector

See Materials and Methods for outline. The original PL451 vector carries a neomycin acetyltransferase resistance gene controlled by two promoters for expression, respectively, in eukaryotic and prokaryotic cells. The neomycin selection cassette is flanked by flippase recognition target (FRT) sites to allow genomic deletion at a later step. It was adapted for use as an AOX entry vector as described, and *Ciona* AOX (Hakkaart et al., 2006), amplified using primers Ciona Aox F AscI, GGCGCGCCACCATGTTGTCTACCGGAAGTAA and Ciona Aox R BamHI, GGATCCCTATTGTCCAGGTGGATAAGGAT (these and all primers shown 5′ to 3′), was directionally cloned using these restriction sites (*Asc*I and *Bam*HI), upstream of the neomycin resistance cassette. The final plasmid, pRosa26-Aox, was produced by cotransformation of this construct with Rosa26 targeting plasmid pRosa26-DTA into recombineering competent *E. coli* (EL250). Following selection for kanamycin resistance and verification by PCR and sequencing, it was used for mouse ES cell electroporation. Correct integration was verified first by negative (DTA) and positive (G418) selection, followed by Southern blotting (Koetsier et al., 1993) using gene-specific restriction enzymes and probes to distinguish the wild-type and manipulated alleles, as shown in Fig. S1B, S1C. Briefly, PCR-amplified 5′ and 3′ probes were labelled with [α-^{32}P]dCTP using the Rediprime II DNA Labeling System (Amersham/GE, Cat. No. RPN1633) according to manufacturer's instructions. Radio-labeled probes were column purified using G50 Quick Spin Columns (Roche) and used to probe Southern blots of genomic DNA from putative positive clones, digested with *Eco*RI for probing with the 5′ probe (manipulated allele 5.8 kb, wild-type allele 15.6 kb) and *Bgl*I for probing with the 3′ probe (manipulated allele 7.5 kb, wild-type allele 6.7 kb). The exact probe sequences were as follows (5′ to 3′).

5′ probe:

CATTAATGGACGCTGCACTGCTGTCCTTCCCTGGAGACAGCAGCCAGCAC
TACTCAAGCTTCTCACGTAGCAACCAGAGCTCCAGAGCCAGCAGCTGCTG
CCGCCTTGTATACTCACTCCTGTGATCCAACACAGGAGCAACCTTTTCTTT
ACCCCACCCCCACTTCTTAACACACTTTTTTTTGGGGGGGGGGGGGGAACA
AGTGCTCCATGCTGGAAGGATTGGAACTATGCTTTTAGAAAGGAACAATC
CTAAGGTCACTTTTAAATTGAGGTCTTTGATTTGAAAATCAACAAATACCA

AATTCCAAATATTCGTTTTAATTAAACCAGCAATGTGGATATAAGCATTAA
GTTTTAGTTTTAAAAAGGTCAATTTTCCAAACATTCAGCAATCATATTTAA
ATTTACAGCTAGGAACAAGAGCCTTGGGTCATG

3´ probe:

ATATTGCTCGCACCAACACAAAAGTTAGTATGTTGCAAAAGACATGCTAT
ATTAAACTCTCTAAAGACAGTATACATTTAAGAAATGTTCTGGACAAACA
CTTCTACATGTCAGTTTTATATATATTATAACACAAACGGTGTTAATTGAA
TAATTAAGCATTTTAAAAGCATGAAACTACAACCATTGTTCATAAATAAG
TTCTAACGTTGTGGTTTTATAATTTGGAACTTTGGGGAAATGTTCAAAACA
TTTTATGACAAACACCTTTATCCTCACATACAAAGAAAGCTACAATACTTA
AAATGGTAATTGCATAACACATTGCATGGATTATACAAGGTGTAACTTAA
GAGTTTAATTCATACAGAACACATATGTTCTACCTACACTACATTAGAAAA
ATCCAAACTGCATAGCAACATTTAACACAGTGACATTACTGTCACTGACC
ATCATGCCTCTGCTTGCTTCTGAGAACATAAATGGCAACATCTTGGGAT.

Full details of metabolomics methods

(i) Metabolite extraction

Approximately 20 mg of skeletal muscle and heart tissue samples were taken from -80 ˚C on the day of analysis and immediately transferred to Precellys homogenization tubes containing 2.8 mm ceramics (zirconium oxide) beads (Bertin Technology, Germany). A total of 20 µl of internal standard mix was added to the samples and equilibrated for 10 min on ice. The extraction was carried out in two steps. First, 0.5 ml of acetonitrile (ACN)+1% formic acid (FA) was added and homogenization was carried out with a Precellys homogenizer (3 cycles of 30 sec, 1 min standing time, 5,500 rpm.). The samples were placed on ice to cool during the standing times. After the first round of homogenization, the samples were centrifuged at 14,000 rpm at 4 ˚C for 15 min in a microcentrifuge and the supernatants were transferred to Eppendorf tubes. The second round of homogenization was carried out by adding 0.5 ml of 90:10 ACN:H_2O + 1% FA and then the same procedure was followed as above. The combined supernatants were centrifuged at 14,000 rpm at 4 ˚C for 15 min and 800 µl of the final supernatant was transferred to an Ostro 96-well plate (Waters Corporation, Milford, USA). The extracts were filtered by applying vacuum at a delta pressure of 400-500 mbar on a Hamilton StarLine robot vacuum station. The clean extract was collected into a 96-well collection plate, which was placed under the Ostro plate. The

collection plate was then sealed and centrifuged for 10 min, 4,000 rpm, 4 °C, and placed in the auto-sampler of the liquid chromatography system for injection.

(ii) Instrumentation and analytical conditions

Sample analysis was performed on an ACQUITY ultra pressure liquid chromatography tandem mass spectrometry (UPLC-MS/MS) system (Waters Corporation, Milford, USA) and the detection system, a Xevo® TQ-S tandem triple quadrupole mass spectrometer (Waters Corporation, Milford, USA), was operated in both positive and negative polarities for measurement of metabolites. A detailed description of the analytical conditions and instrument parameters has been published elsewhere (Roman-Garcia et al., 2014).

(iii) Metabolomics data analysis

Metabolomics data analysis was carried out using a web-based comprehensive metabolomics data processing tool, MetaboAnalyst 2.0 (http://www.metaboanalyst.ca, Xia et al., 2009, 2012). The non-transformed data was autoscaled i.e., mean-centered and divided by standard deviation. Dendrograms were plotted using Ward's linkage clustering algorithm and Pearson's correlation similarity measure. In order to explain the separation among groups, unsupervised multivariate regression technique, principal component analysis was performed.

Respirometry on tissues from *AOX*^{Rosa26} founder mouse

Mouse tissues were processed, mitochondrial pellets resuspended and mitochondrial protein assayed as described in Materials and Methods. Oxygen consumption was measured with a Hansatech Oxytherm unit. For each assay, mitochondria equivalent to 75 mg of protein were transferred into respiration buffer (225 mM sucrose, 75 mM mannitol, 10 mM Tris/HCl, 10 mM KCl, 10 mM KH_2PO_4, 5 mM $MgCl_2$, 1 mg/ml BSA), which was pre-equilibrated at 37 °C. Oxygen consumption was measured by the successive addition, to final concentrations, of complex II substrate mix (10 mM sodium succinate + 1 mM ADP in the presence of 150 nM rotenone), cIII inhibitor (30 ng/ml antimycin A) and AOX inhibitor (200 µM n-propyl-gallate).

Respirometric titration of antimycin inhibition

Heart mitochondria were prepared as for ROS measurement. Oxygen consumption of aliquots containing 100 µg mitochondrial protein was measured using an O2k oxygraph (Oroboros) in 5 mM $MgCl_2$, 120 mM mannitol, 20 mM MOPS, 5 mM

KH_2PO_4, 60 mM KCl, pH 7.4, using a multiple substrate inhibitor protocol as described previously (Gizatullina et al., 2011), using increasing amounts of antimycin A.

Submitochondrial fractionation

To analyze membrane association of AOX, 500 µg of mouse liver mitochondria were suspended in 500 µl 10 mM Hepes/KOH, pH 7.4, and an equal volume of 200 mM sodium carbonate solution was added (final pH adjusted to 9.5 with HCl). After thorough mixing, samples were incubated on ice for 30 min and then centrifuged at 230,000 g_{max} in a Beckman TLA120.2 rotor for 1 h at 4 °C. The pellet containing the membrane fraction was dissolved in 60 µl SDS-PAGE sample buffer. The supernatant fraction was precipitated on ice for 30 min by the addition of 150 µl of 100% (w/v) trichloroacetic acid, pelleted at 20,000 g_{max} for 30 min at 4 °C, washed twice with ice-cold acetone, air dried and resuspended in 60 µl SDS-PAGE sample buffer. One-third of each fraction was electrophoresed on SDS-12% polyacrylamide gels, and processed for Western blotting and probing with AOX and OXPHOS subunit antibodies as described in Materials and Methods.

Western blotting of mitochondrial protein extracts from brain

To study the expression of AOX in brains of newborn or young mice, and according to gene dosage, a slightly variant procedure was used for protein extraction. Washed tissue was snap-frozen in liquid nitrogen, then placed into 400 µl of RIPA buffer (Sigma) containing Pierce™ protease inhibitor (ThermoFisher Scientific) in Eppendorf tubes and crushed on ice with a chilled mortar and pestle. Frozen tissue pieces were transferred to a fresh tube and a further 450 µl of the same buffer solution added. The tissue was further disaggregated using scissors and a plastic grinding rod for use with Eppendorf tubes, left on ice for 30 min, then centrifuged at 14,000 g_{max} for 5 min at 4 °C. The supernatants were collected, their protein concentration determined by the Bradford method, and 20 µg aliquots used for SDS-PAGE and Western blotting via standard methods. Blots were probed for AOX using the customized antibody (1:10,000) and were stripped and reprobed for GAPDH (rabbit antibody, Cell Signaling 2118, 1:1,500), in both cases detected using anti-rabbit secondary antibody (see main Materials and Methods).

SUPPLEMENTARY REFERENCES

Gizatullina, Z. Z., Gaynutdinov, T.M., Svoboda, H., Jerzembek, D., Knabe, A., Vielhaber, S., Malesevic, M., Heinze, H.J., Fischer, G., Striggow, F. and Gellerich F.N. (2011). Effects of cyclosporine A and its immunosuppressive or non-immunosuppressive derivatives [D-Ser]8-CsA and Cs9 on mitochondria from different brain regions. *Mitochondrion* **11**, 421-429.

Roman-Garcia, P., Quiros-Gonzales, I., Mottram, L., Lieben, L., Sharan, K., Wangwiwatsin, A., Tubio, J., Lewis, K., Wilkinson, D., Santhanam, B., et al. (2014). Vitamin B12–dependent taurine synthesis regulates growth and bone mass. *J. Clin. Invest.* **124**, 2988-3002.

Xia, J., Mandal, R., Sinelnikov, I., Broadhurst, D. and Wishart, D.S. (2012) MetaboAnalyst 2.0 – a comprehensive server for metabolomics data analysis. *Nucleic Acids Res.* **40**, W127-133.

Xia, J., Psychogios, N., Young, N. and Wishart, D. (2009). MetabSoAnalyst: a web server for metabolomics data analysis and interpretation. *Nucleic Acids Res.* **37**, W652-660.

SUPPLEMENTARY FIGURES

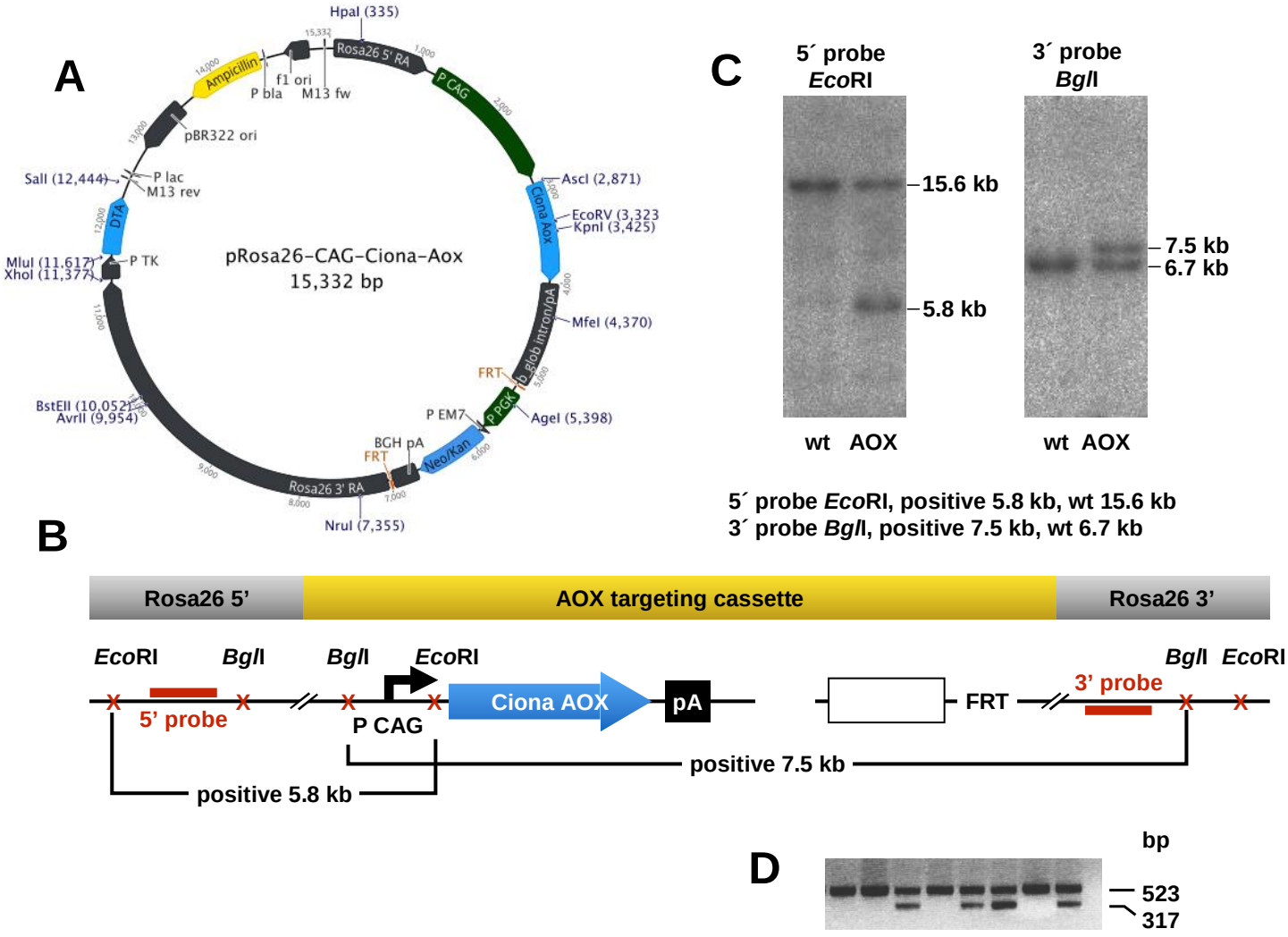

Figure S1

Supplementary Information on Rosa26-AOX construct and expression

(A) Full map of Rosa26-AOX targeting construct. (B) Schematic map of mouse *Rosa26* locus, showing relevant restriction sites for verifying insertion of AOX targeting cassette (other non-relevant sites in insert omitted for clarity). Note that the FRT-flanked PGK-neo selection cassette was excised *in vivo*, following first germline transmission of the modified allele. (C) Southern blot of DNA from selected ES cells positive for targeted AOX insertion, alongside parental (wt) cells, digested and probed as indicated. Fragment sizes, estimated from markers, correspond with those predicted for the insertion as shown in (B). (D) Sample multiplex PCR for genotyping of mice according to the scheme described in Materials and Methods: 523 bp product is from the wild-type *Rosa26* allele, 317 bp product is from AOX.

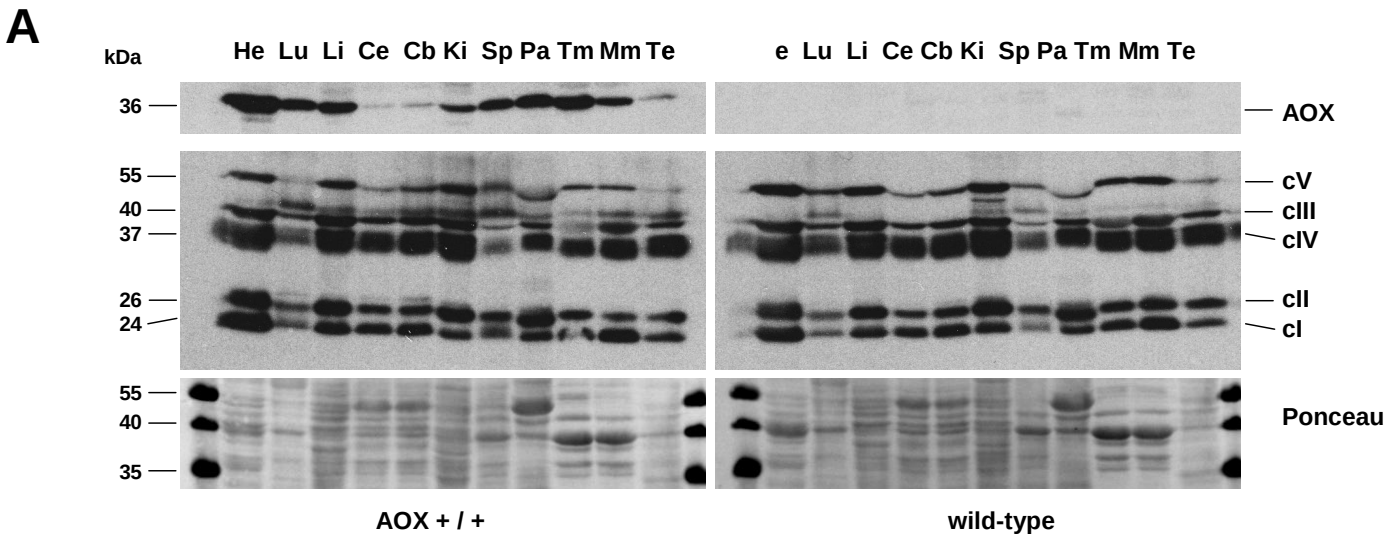

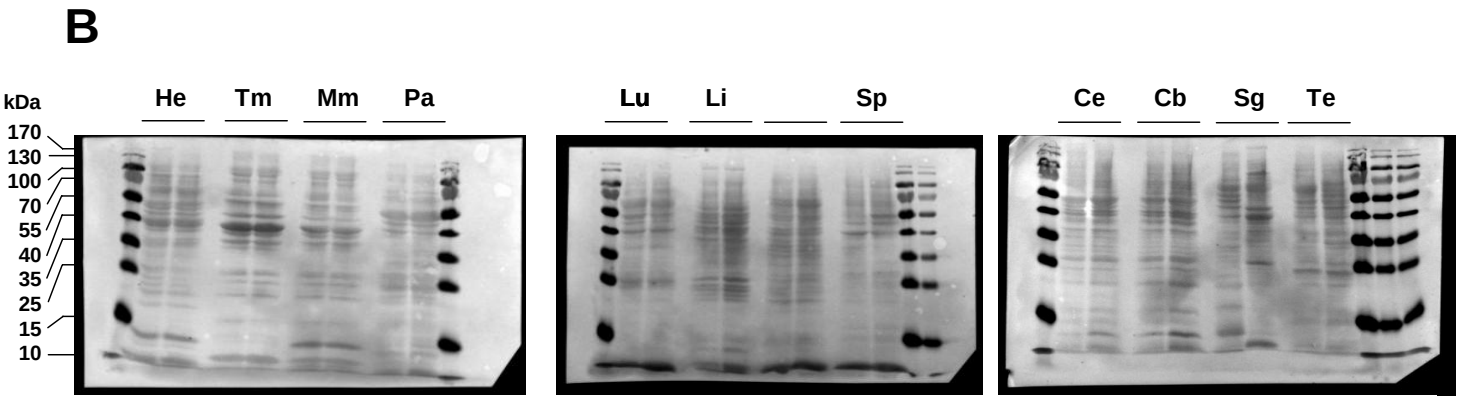

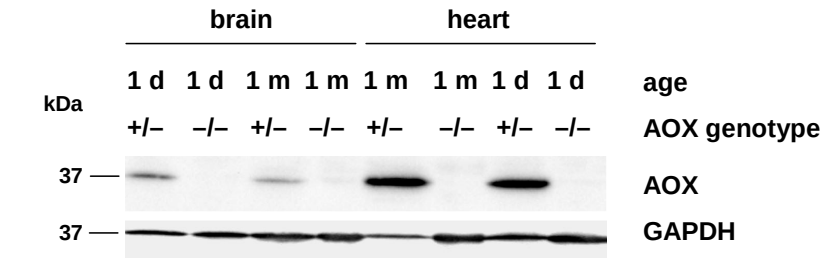

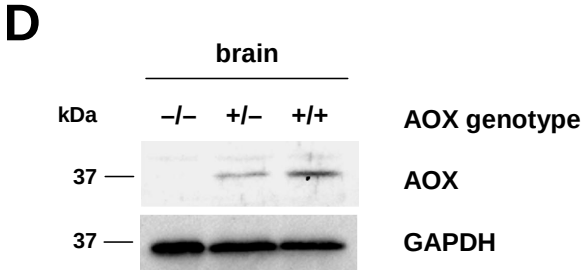

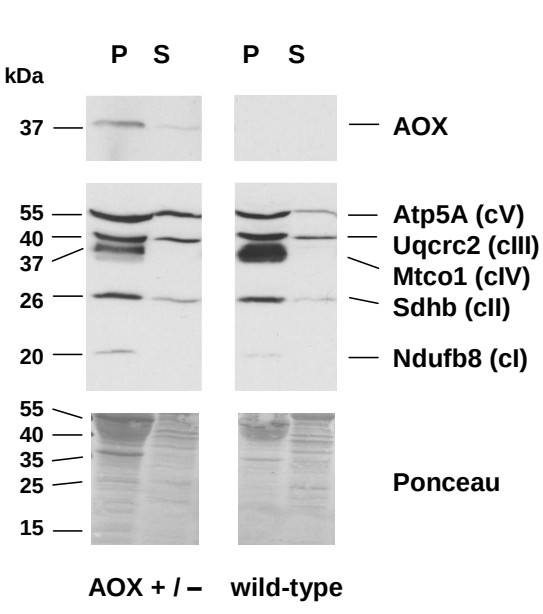

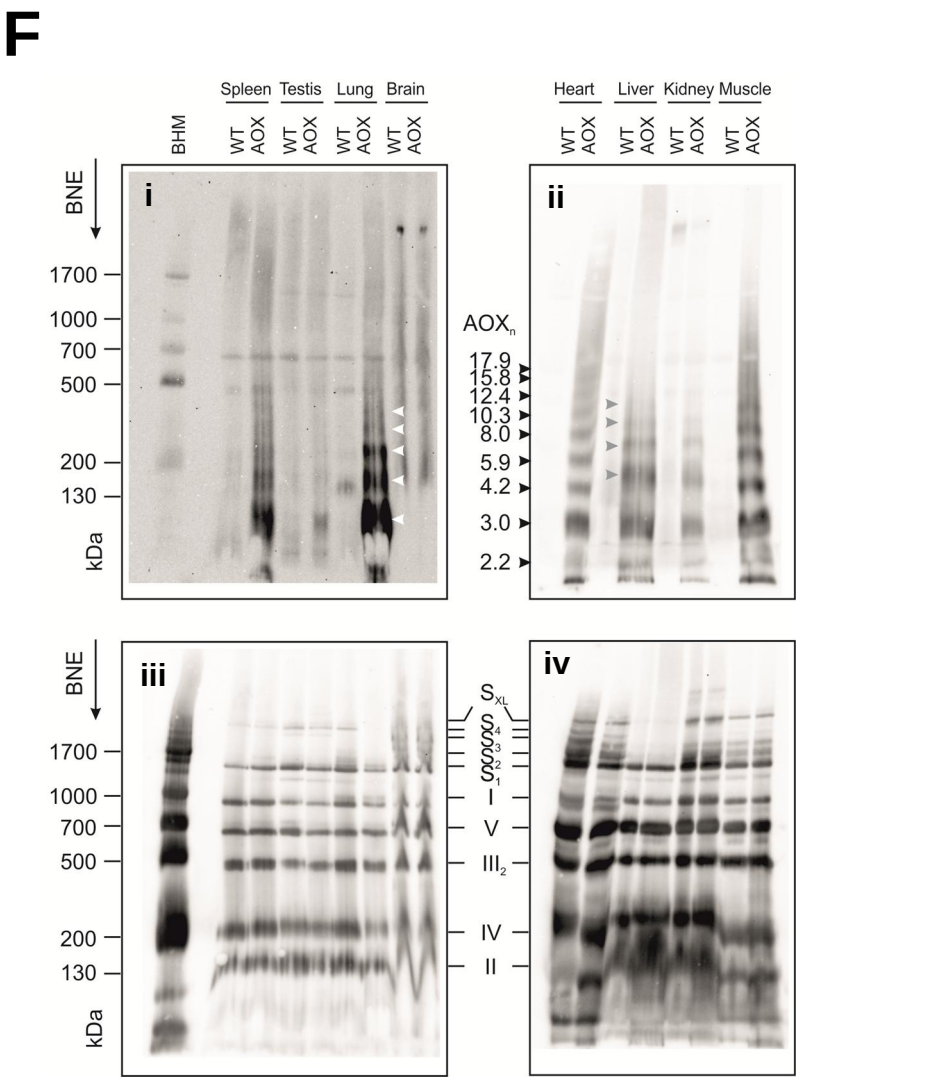

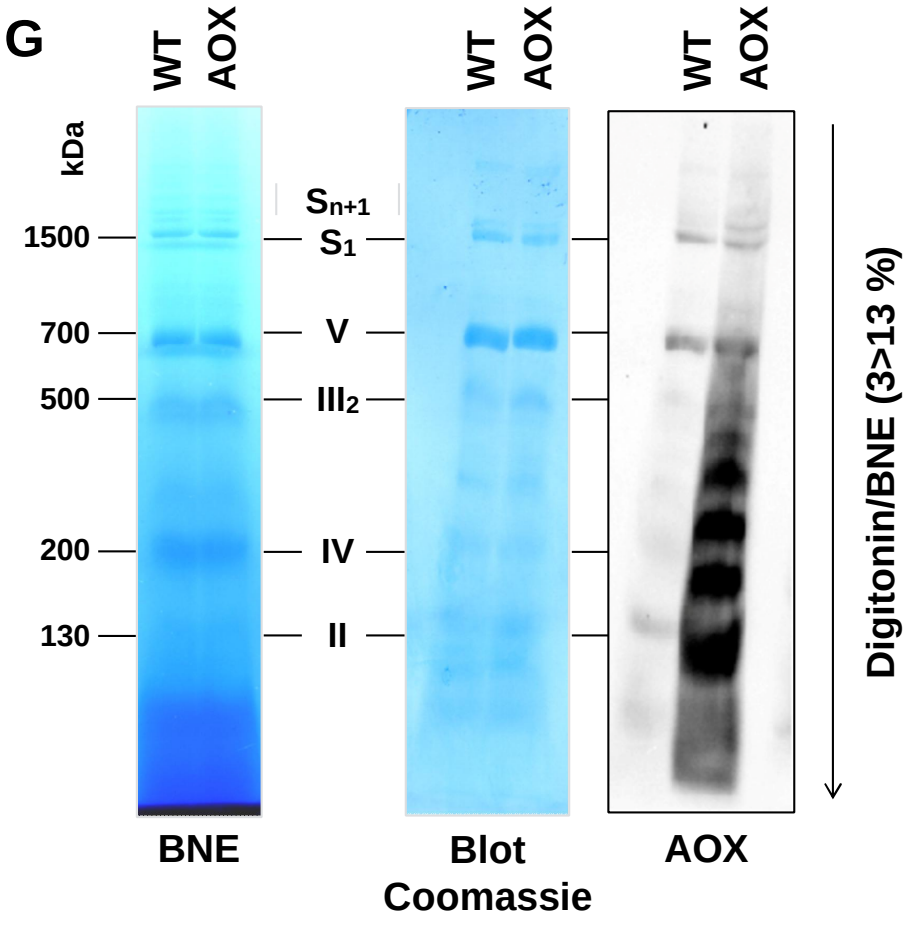

H

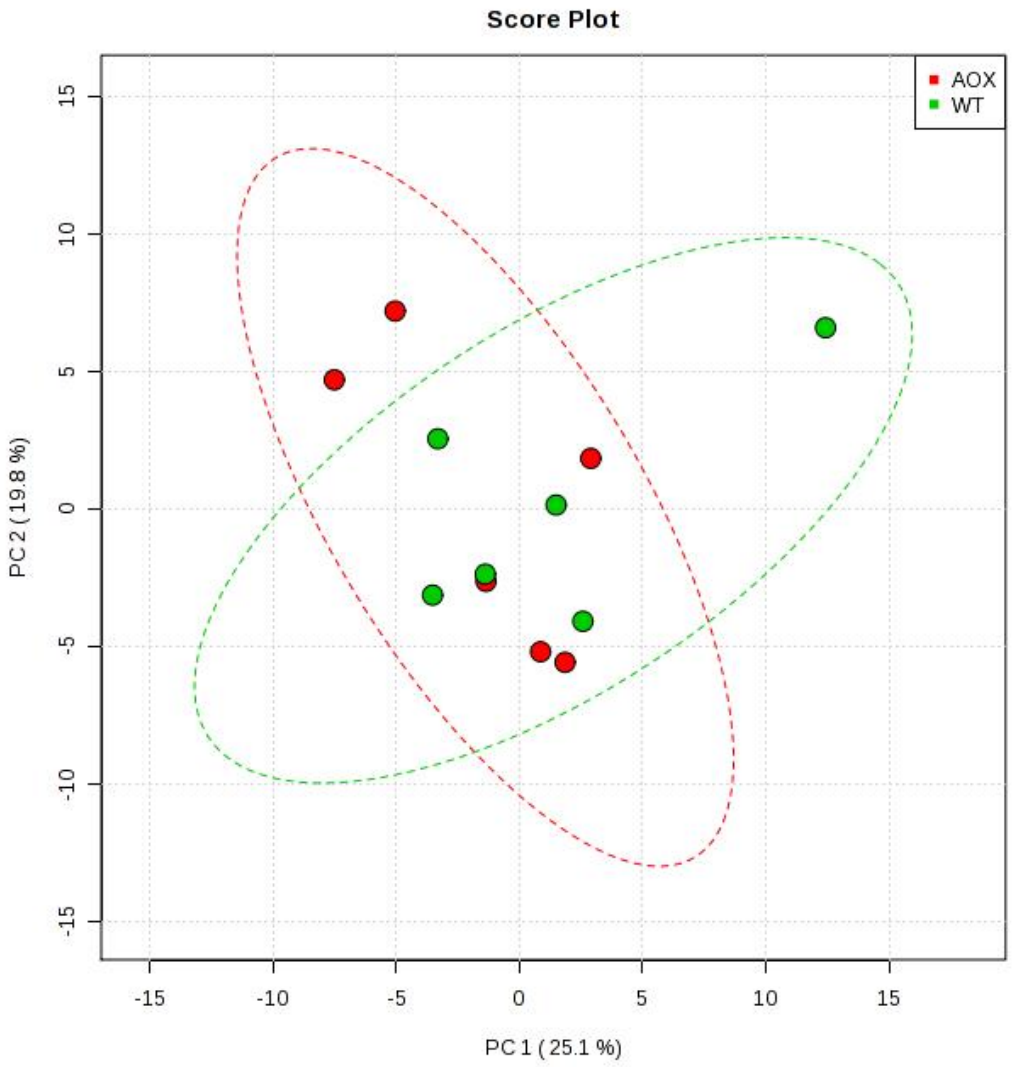

Figure S2

Supplementary data on protein expression and biochemistry of *AOX*^{Rosa26} mice (A) Western blots of 20 µg total protein extracts from the indicated tissues (He - heart, Lu – lung, Li – liver, Ce – cerebrum, Cb – cerebellum, Ki – kidney, Sp – spleen, Pa –pancreas, Tm – thigh muscle, Mm – masseter muscle, Te – testis) of 24 week-old male hemizygous *AOX*^{Rosa26} (+) and wild-type littermate control (–) mice, probed for AOX and for representative subunits of the five OXPHOS complexes (see Materials and Methods; protein molecular weights extrapolated from markers). Ponceau S staining of the membranes is shown below, including actual molecular weights of markers. (B) Ponceau S staining of the blot membranes from the experiment shown in Fig. 2A. Molecular weights of markers as indicated. (C, D) Western blots of 20 µg aliquots of total protein extracts brain and heart of one-day (1d) and one-month (1m) old hemizygous (+/–) and homozygous (+/+) *AOX*^{Rosa26} and wild-type littermate control (–/–) mice, probed for AOX and for GAPDH as a loading control. Protein molecular weights extrapolated from markers. (E) Western blot of carbonate-extracted proteins from liver mitochondria of hemizygous *AOX*^{Rosa26} (+/–) and wild-type littermate control mice, probed for AOX and representative subunits of the OXPHOS complexes as indicated. Ponceau S stained membranes are shown below. The cropped images are from nonadjacent tracks of the same gel. AOX co-fractionates with the

more tightly membrane-associated pellet (P) than supernatant (S) fraction. Protein molecular weights extrapolated from markers and as shown for Ponceau S-stained image. (F) Complexes of OXPHOS and AOX in mouse tissues, as indicated. Mitochondrial complexes from mouse tissue were isolated by BNE (3 to 13% acrylamide gradient gels) and PVDF blots were probed with an antibody against (panels i and ii), AOX and (panels iii and iv), an antibody cocktail against rodent OXPHOS complexes (Mitosciences) and complex IV (rabbit antiserum). Assignment of mitochondrial complexes I, cI; III_2, dimeric cIII; IV, cIV; V, cV; $S_{0\text{-}1}$, respiratory supercomplexes containing cI, dimeric cIII and 0 or 1 copy of cIV; S_{XL}, larger supercomplexes; wt, wild-type; AOX, male hemizygous *AOX*^{Rosa26} mouse. Black arrows indicate AOX oligomers of heart and muscle tissue, grey arrows indicate AOX oligomers of liver and kidney, white arrows are the markers for lung. Bovine heart mitochondria (BHM) as molecular weight ladder. Note: AOX appears in high molecular complexes (panels i and ii). When reprobed for OXPHOS complexes (panels iii and iv), AOX-containing tissues exhibit a similar migration pattern as controls, which also differs from the ladder of AOX multimers. Thus, it can be inferred that AOX does not form heteromers with endogenous complexes. Furthermore, the molecular weights of each OXPHOS complex from mouse were used for exponential regression. Apparent molecular weights of AOX complexes were divided by that of the AOX monomer to infer the stoichiometry of AOX homo-oligomers. AOX oligomers from tissues other than heart and muscle seem to have a slightly decreased mobility, which may reflect different solubilization behaviour determined by lipid/protein content rather than additional or altered polypeptides. (G) Western blot of BNE gel of extracts from heart mitochondria of hemizygous *AOX*^{Rosa26} (AOX) and wild-type littermate control (WT) mice, probed for AOX, alongside Commassie Blue stained blot (CB); protein molecular weights extrapolated from bovine heart mitochondrial extract, used as marker. Complexes and supercomplexes denoted as in part (F). Note the faint bands in the control track, which are non-specific cross-reaction to complexes with high protein content. (H) Principal component analysis of metabolome data from heart of hemizygous *AOX*^{Rosa26} (red circles) and wild-type littermate control mice (green circles). The two sets of analyzed data largely overlap. Both for heart (here) and skeletal muscle (Fig. 2C), none of 100 individual metabolites analysed showed a significant difference between *AOX*^{Rosa26} and wild-type samples, nor was any significant alteration seen in any specific metabolic pathway.

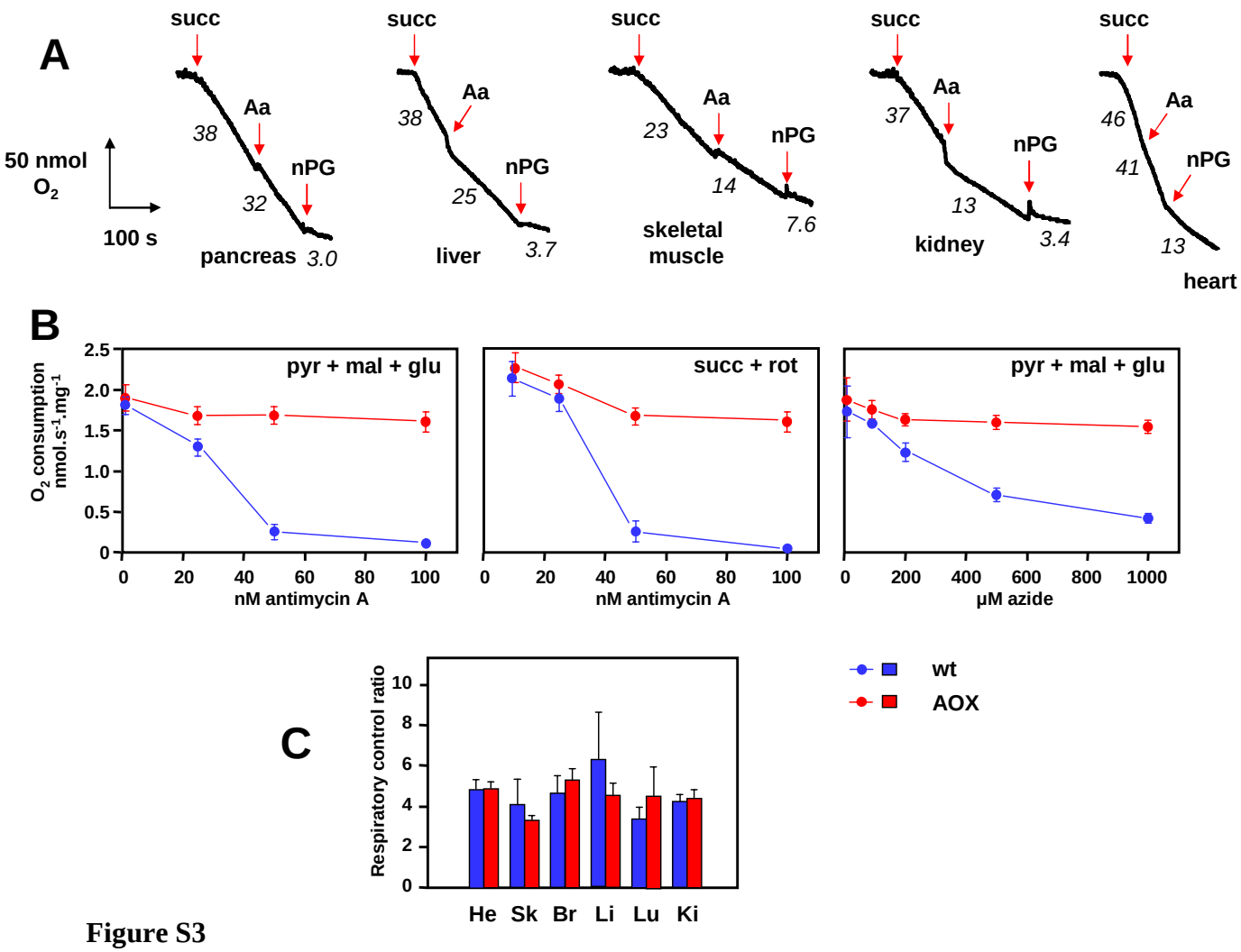

Figure S3

Supplementary data on functionality of AOX in *AOX*^{Rosa26} mice

(A) Oxygraph traces for mitochondria isolated from indicated tissues of hemizygous *AOX*^{Rosa26} founder mouse (i.e. in the generation after removal of neomycin-resistance cassette), according to the scale arrows shown left. Red arrows indicate times at which substrate mix (succinate), and inhibitors (Aa – antimycin A, nPG – n-propyl gallate) were added. Rates of oxygen consumption estimated from slope (2 significant figures, nmol O_2/min), shown in italics. (B) Respirometry of isolated heart mitochondria from wild-type and hemizygous *AOX*^{Rosa26} mice as indicated, using the substrates and inhibitors shown (pyr + mal + glu – pyruvate, malate and glutamate mix, succ + rot –succinate plus rotenone). Means + SD for at least three biological replicates in each case. (C) Respiratory control ratios (means + SD) for the mitochondrial preparations analysed in Fig. 3A, computed from the raw data of the same experiment. RCR is here defined as the ratio between (oxygen consumption in the presence of the cI-linked substrate mix and ADP, minus the residual value after addition of rotenone, i.e. state 3) and the oxygen consumption in the presence of the cI-linked substrate mix alone (i.e. state 2). RCR values for *AOX*^{Rosa26} and control mouse mitochondria showed no significant difference for any tissue tested (Student's *t* test, $p > 0.05$).

TABLE S1. Skeletal Muscle

Units: µmoles		AOX						WT					
Metabolite name	**Comments**	**1_MS 213**	**2_MS 214**	**3_MS 216**	**4_MS 223**	**5_MS 240**	**6_MS 250**	**7_MS 215**	**8_MS 224**	**9_MS 230**	**10_MS 241**	**11_MS 267**	**12_MS 234**
Taurine		24951.13053	25315.94534	29063.92645	27875.00513	12775.3621	20411.17992	26882.32798	24656.83866	25621.3959	32078.11205	23454.37812	23481.75411
Glutamine		12081.4761	13960.58762	13443.09022	14114.92002	7113.424603	11675.39854	12762.98351	14323.11595	15724.58653	17937.06621	16178.03345	11346.74184
Alanine		11407.65021	12770.46736	16562.27884	11091.72394	11635.38867	6909.695656	13209.95126	10502.2386	9460.590527	10584.43165	8735.516242	10692.50454
Creatine		10290.2817	10032.5741	11713.91755	10788.52587	5616.77699	8580.13063	10980.6713	10804.27782	10711.89475	11667.22933	9469.193486	9889.103621
Glycine		4035.658746	6748.686574	4735.09206	4920.037614	4007.101341	2505.13554	5099.157656	3724.328496	2470.835255	3721.006715	4164.811592	2412.001712
Acetoacetic acid		2151.485225	2264.083573	2462.5374	2104.720148	2171.343369	1672.0095	2058.228515	2051.513935	2021.842174	2348.261927	1803.00762	1791.462188
Cysteine	>ULOQ	1660.880676	1687.258938	1869.851877	2010.66042	1626.899064	1271.10979	1751.490675	1766.622845	1725.966854	1827.635012	1880.607567	1326.187261
Hydroxyproline		1512.122973	2132.732086	2203.792248	1828.877868	1552.040798	1039.471893	1996.288627	1797.972067	1450.576291	1506.502876	1288.156442	1371.946975
Lysine		892.6431464	1059.506372	1313.938631	970.9061662	1029.296838	716.8049012	1033.060829	931.492463	524.5103317	833.4631824	517.3812381	774.5929945
Threonine		661.5861113	738.3451812	792.1129829	745.4534668	521.7794118	311.5564203	729.1747116	586.3684718	413.4210178	606.1831435	526.3516277	537.2041313
Niacinamide		552.9037212	537.511418	667.6601992	564.3336493	292.1489618	395.9327088	498.3448645	491.3345086	547.1125576	680.3093196	502.6120376	475.6374074
Serine		550.2364065	621.5547131	618.084121	568.6222813	497.3511936	242.3335029	589.5697836	525.7710931	383.8073498	472.3664719	543.2834176	466.8477583
IMP		456.4934028	461.0127338	651.797263	453.0357672	509.095423	329.16477	420.5899277	457.5479728	481.6463211	811.6394273	514.9953143	393.4632535
Creatinine		429.5786885	482.2018722	656.0568944	375.2280868	531.0960266	328.4397372	682.8181633	365.5874494	465.5528533	269.5649456	336.8245692	471.5851065
D-Ribose 5-phosphate		426.5352689	473.4950112	593.5224089	414.165951	420.4462976	253.1330109	483.8751034	444.7940965	394.4731558	534.0936179	432.0797638	311.8205593
Hypoxanthine		399.3766089	615.6771208	484.420173	474.8493539	212.1987323	304.6254997	404.9823744	352.6163212	400.8805947	697.9861651	991.6735858	213.9761701
Valine		383.8706178	361.8939998	424.7524229	360.8878414	338.4558043	202.8786056	391.0302293	299.0143944	241.1496943	331.2061681	303.4944471	276.3122832
Proline		372.0377227	493.1837017	457.7230564	410.9846219	366.4284639	201.7393343	462.2330944	384.5925477	276.7342076	414.023644	397.9879533	336.3561556
Leucine		363.6536308	313.9286364	460.4031279	353.4381098	383.6353791	188.6371628	396.6412508	267.637192	283.9347316	318.4263033	271.9409532	245.1157517
Glutathione		349.7905121	253.3634133	393.0979088	247.3670046	177.0454834	217.0821117	205.149864	268.5664295	170.8067955	390.6145476	290.189843	316.174281
Arginine		319.1592909	385.773662	595.6550451	430.9227298	403.1260878	298.042959	432.5892464	355.0748597	202.3393273	308.9358526	255.1515226	284.0306881
Carnitine		229.6966291	215.2381257	286.2799073	248.5423282	226.2830831	147.9600962	296.1280069	199.2094681	207.9145878	184.15446	194.8838471	166.1477159
L-Methionine		223.4854344	210.8941784	283.5507586	220.9480488	212.6162729	99.04954984	257.760938	182.0886126	165.1588433	185.4995244	193.8520986	159.0524793
Myoinositol		215.783903	171.28013	163.2195241	193.1377665	152.0393499	148.4308428	211.4523172	167.0001927	136.5448062	308.0074275	155.4619225	94.39620387
Histidine		214.587819	193.8331215	183.4057952	185.2169834	180.3391697	120.9018102	211.8650394	143.3797354	154.9905312	190.9823992	145.6187318	171.6910459
Tyrosine		201.7156553	185.8932755	241.2835891	215.1069836	197.0281769	112.9000934	207.8412207	159.1380112	131.1261328	174.4091244	240.629602	157.5116034
Glyceraldehyde		200.7610809	216.5517425	254.7234117	210.5880648	196.9459799	86.78321755	233.4924436	163.9529316	140.621592	185.9827294	241.1364185	134.9540322
L-Glutamic Acid		190.8530195	208.9361397	174.3678249	218.1273736	184.111376	114.1736755	194.9932909	159.3329901	123.4829619	193.6272543	169.928206	143.2483308
Phenylalanine		178.4219904	169.9827572	224.7983373	186.4781342	170.7789821	89.38376097	193.9521325	153.0930234	124.7932361	159.8233776	197.0957186	127.9330665
Isoleucine		178.3223242	197.8027552	220.2674427	206.3960894	187.0811876	101.0106935	191.7018191	158.0331644	123.6882043	182.8530969	155.9238484	128.9804117
Inosine		158.0084182	193.839633	188.6313521	134.7885514	160.7860138	83.93149259	147.9272031	113.2662327	173.0573896	216.6131418	386.4997707	65.35328642
Choline		153.1128352	207.9618905	220.1108669	195.4555912	47.16661434	125.7776382	146.1450399	136.6759847	115.9512602	231.1878748	274.0666151	177.5894494
Aspartate		141.1290738	119.8499617	107.8728881	116.2381983	128.3690631	132.0600523	142.72291	149.9044939	88.64432561	125.2000319	81.50002451	154.4949287
Acetylcarnitine		137.7263929	174.9051931	167.8540413	128.5690529	57.8743885	86.35371576	127.5617455	143.0376501	183.1467991	158.2388344	134.3381771	100.1812991
Ornithine		127.1355592	120.4797879	151.0033994	131.1722048	109.538601	69.42560941	144.4368097	129.299389	126.6051628	114.5186951	141.1558618	111.9652821
Citrulline		112.8031205	148.7151414	137.8622185	124.2686228	117.3850723	88.56551625	127.798921	126.6764491	93.26431842	159.4972459	118.1251248	108.3486419
Phosphoethanolamine		111.079288	163.5743087	201.6222073	136.7156754	168.2038947	51.47941354	206.5727428	144.5767388	100.6945946	212.2970742	119.3052665	82.40047558
Asparagine		104.8596237	120.1045058	121.381564	99.78425638	96.01881274	70.21942024	108.3011077	97.81702335	68.5526715	91.12655305	136.9081502	97.21135973
Allantoin		71.69206452	63.44208303	68.03194435	66.29407378	65.29371939	43.59583655	75.25411074	77.07436343	44.91787353	79.51052059	57.00843128	40.91253302
Carnosine		71.07444545	64.24669201	88.43174637	78.31350934	47.54748781	66.87907888	72.96647351	79.30065442	58.15929738	96.65795533	65.56288545	95.67081026
Cholic Acid		70.00306233	80.98208878	85.72144446	69.86335687	66.21582969	39.18434283	83.50741672	68.70319419	59.24726089	60.94954148	59.28218725	59.32622484
Xanthine		59.4171945	99.06807866	99.78989358	57.66363283	76.48383548	41.63281666	78.00087023	60.49787786	63.15676673	91.0383974	92.11092466	39.81400617
Tryptophan		33.9725821	37.91574686	42.85533539	38.25295125	36.60338386	25.71259366	37.72132271	32.58731004	22.03068634	35.88036906	38.98507968	31.08356076
Betaine		30.53426013	32.13881802	44.47220197	49.62479217	42.56579655	13.63609432	34.31529754	41.05655892	43.37072328	31.82108378	93.48800351	32.89608462
Succinate		25.20414655	20.08242023	22.10484549	11.8561398	11.78259706	10.4693339	41.82480509	9.339927586	14.86613896	27.65732213	23.67025518	9.875738955
GABA		22.25214298	26.03001424	14.01662426	10.46133459	7.002296413	3.753808386	16.36877022	17.7223069	17.40948954	12.78340196	47.58433387	6.755651952
Sorbitol	bad chromatography and unreliable values	22.15367556	17.57379643	18.31270629	19.53854755	93.6236258	339.1664393	25.75288168	22.61677114	123.7384593	135.2817978	156.3969134	223.4674555
Pantothenic Acid		14.12263479	17.41914241	18.26519888	12.95966086	19.51306142	9.716916025	17.22955786	16.36935329	15.26297176	20.14689636	12.67386921	12.67669883
Aminodipic Acid		10.431567	8.518471504	11.20527363	6.027982998	10.94352214	5.839367949	7.128878999	11.02435716	3.129470101	7.498410524	14.40788018	6.516842411
deoxycytidine		10.22182305	7.33874475	8.029482259	7.406999445	8.215135028	8.247897281	6.937407147	7.832908738	8.449931177	8.739331081	8.832157466	6.727182688
Chenodeoxycholic Acid	bad calibration and low response	9.206136977	4.200843277	6.299684462	8.667202607	11.5610115	20.40048345	6.987181387	27.40979118	14.33786689	13.57134733	9.081281214	10.51159091
Homocysteine		9.058809764	10.01840999	11.56570796	12.47021151	8.668541731	4.848506392	9.462851963	8.218585645	6.138686596	5.78974106	7.59874818	7.745672616
Homoserine		8.201868055	7.181191142	7.717567275	5.191912667	4.910705763	3.968141878	4.093122725	4.624291323	5.504364784	7.264511706	6.316740287	3.655689762
DimethylGlycine		7.700119767	6.569164676	8.037000007	9.510851056	5.480319616	3.892169914	10.46735031	8.199424408	5.414146711	3.579352548	9.552961086	7.050422162
AMP		7.624435304	14.21810698	11.42236161	6.486486549	6.625827213	8.84991858	7.615503211	8.742733454	6.581166744	18.23576279	13.38384941	7.971000545
Xanthosine	minor concentrations	7.005879461	4.157694821	4.548365357		2.538267232	0.803166244	3.804127072	2.184699483	2.141049144	3.701548775	6.781080214	
S-5-Adenosyl-L-Methionine		5.444094112	2.024329956	4.84612196	1.413605352	2.356190474	13.45734726	1.564730198	3.030956652	2.590254264	10.8220483	1.190377219	1.335344926
Guanosine		3.760407296	2.516428645	2.109069438	1.360054124	1.37757495	1.38414526	1.865967977	1.305301542	1.462988977	2.212004292	3.988178035	0.58475757
Uracil		3.575200771	5.62845075	5.191235795	4.831501971	5.534366519	3.254207513	3.940468962	4.792761406	2.335502671	4.947723668	13.29354838	1.372522897
Asymmetric dimethylarginine		3.352379671	4.306258973	3.4996022	5.103714339	4.241849117	1.723730444	5.321480996	3.18368719	1.920027149	3.981142555	3.097807381	2.303419152
Guanidinoacetic Acid		3.066794272	3.765959805	2.505343162	2.378222155	2.976750226	1.700243456	2.653651002	1.816771045	1.223539684	5.296708587	5.174884289	1.87503484
Symmetric dimethylarginine		2.97512194	3.910598427	4.10076086	3.671361817	2.876973588	2.085652494	3.070203157	3.855389978	1.754401804	2.481313041	1.969101325	2.128592399
Cytidine		2.349049774	3.058100629	2.749484969	1.956266207	2.088894425	1.787930393	2.94332621	2.206219386	2.956078923	1.642549462	1.831289618	1.946064037
Trimethylamine-N-Oxide		2.18867022	2.510776403	3.510131485	2.403407676	1.949155366	1.73441791	2.998065245	3.939606396	2.742032125	2.742032125	1.651826581	1.205833404
Taurocholic Acid		1.919107226	2.425655277	2.120041964	1.654402781	1.739830125	1.587023468	1.941968064	1.81442865	2.231939752	1.360821488	1.824054266	1.544911397
Propionylcarnitine		1.52764633	0.870901179	1.293502406	0.825214559	1.153587135	0.985117727	1.11932217	0.845202455	1.167864203	0.876612006	1.062213896	0.850913283
UDP-Glucose	mostly ND	1.238784232		0.696610762		0.955101548	4.752506441				3.064649233		
Hippuric acid		1.16688289	0.671736738	1.087243998	0.588635286	0.89334061	0.786001234	2.454955397	0.997217425	0.370493974	0.869102686	1.232671539	0.498608712
S-Adenosyl-L-Homocysteine		1.098495613	1.386215292	1.405406611	0.975822894	1.106359373	0.948833991	0.922658582	0.922560123	1.093204685	2.163102166	1.44268361	0.842258414
Sucrose		0.810075615	0.251902708	0.208408715	0.413192931	0.306270199	0.592605651	0.603479149	0.248278209	0.065240989	0.458499174	0.197535217	0.081551236
Neopterin		0.808436505	0.911328424	1.080365148	0.764339968	0.80353689	0.583054207	0.933376692	0.810886313	0.79373766	0.754540738	0.705544586	0.676146895
1-methylhistamine		0.73352077	1.298530011	1.060631383	0.916900962	0.941682069	0.579877906	0.827688977	0.73352077	0.723608327	0.902032298	0.911944741	0.59474657
NAD		0.696443608	0.693642897	1.234180228	0.672170775	0.910231257	0.812206353	0.656300076	0.389298907	0.684307191	1.546926352	0.813139923	0.374361779
Adenosine		0.603526645	0.907611224	0.963321376	0.626739208	0.696376898	0.835652278	0.759050819	0.89136243	0.721910718	1.195447008	1.752548527	0.680128104
2-Aminoisobutyric acid		0.535398953	0.601571857	0.776027695	0.667744761	0.553446108	0.330864521	0.643681887	0.595556138	0.487273204	0.451178893	0.613603294	0.517351797
3-OH-DL-KYNURENINE	ND or <LLOQ	0.509104546		0.43716586	0.138343627		0.190914205	0.154944862	0.558908251	0.121742391	0.376294664		0.489736438
Glycocholic Acid		0.434377967	0.245170386	0.313125222	0.241173043	0.289141162	0.257162416	0.270486894	0.229181013	0.294470953	0.218521431	0.377082714	0.215856536
cAMP	<LLOQ	0.420176085	0.406986701	0.486123004	0.382492131	0.388144724	0.2449457	0.478586213	0.382492131	0.459744236	0.499312388	0.299587433	0.316545212
Cytosine		0.407588902	0.340587987	0.385255263	0.212169565	0.268003662	0.307087529	0.195419337	0.340587987	0.323837758	0.424339131	0.29592071	0.245670023
3-Hydroxyanthranilic acid	ND or <LLOQ	0.388911356				1.446264104			1.968863739	1.340933945	1.421957145	0.324092796	

Units: µmoles		AOX						WT					
Metabolite name	**Comments**	**1_MS 213**	**2_MS 214**	**3_MS 216**	**4_MS 223**	**5_MS 240**	**6_MS 250**	**7_MS 215**	**8_MS 224**	**9_MS 230**	**10_MS 241**	**11_MS 267**	**12_MS 234**
L-Kynurenine		0.32477145	0.235384813	0.378403433	0.333710114	0.241343922	0.25326214	0.294975904	0.29199635	0.309873677	0.381382987	0.286037241	0.36350566
Octanoylcarnitine		0.304376953	0.38424892	0.654086644	0.58932559	0.38424892	0.356185796	0.567738572	0.684308469	0.248250706	0.310853059	0.371296709	0.453327377
Cystathionine		0.301530037	0.245691141	0.329449484	0.351785043	0.318281705	0.184268356	0.337825319	0.382496435	0.209395859	0.435543386	0.178684466	0.234523362
Hexanoylcarnitine		0.29662972	0.528670711	0.641102944	0.586082915	0.418630654	0.339688873	0.543023762	0.590867266	0.349257574	0.43537588	0.387532377	0.385140201
Palmitoyl Carnitine		0.157378994	0.19860159	0.163659187	0.185320807	0.133532892	0.176865447	0.220555095	0.379187023	0.192770093	0.503697863	0.09010563	0.19522162
Folic Acid	interfering peak and folic acid could be under that; integrated as a shoulder, unreliable values	0.120868746	0.299360965	0.158815911	0.244548394	0.189735823	0.12930145	0.198168526	0.122274197	0.243142943	0.112436043	0.167248614	0.18130312
Taurochenodeoxycholic Acid		0.094372735	0.064570818	0.086922256	0.052153353	0.04966986	0.068296058	0.110515439	0.055878593	0.08195527	0.093130988	0.151493074	0.054636846
Decanoylcarnitine		0.086536976	0.078669978	0.151439708	0.151439708	0.165206954	0.194708196	0.155373207	0.237976684	0.084570227	0.098337473	0.114071468	0.241910183
Normetanephrine		0.077885389	0.098203317	0.094816996	0.067726425	0.067726425	0.060953783	0.08127171	0.064340104	0.077885389	0.104975959	0.067726425	0.067726425
Isovaleryl Carnitine		0.073339051	0.025289328	0.080925849	0.030347193	0.025289328	0.01770253	0.053107589	0.030347193	0.032876126	0.09104158	0.06322332	0.048049723
2-deoxyuridine	ND and minor values	0.070678624	0.127765205	0.372421981		0.106017936				0.065241807	0.067960216		
Isobutyryl Carnitine		0.059010051	0.053645501	0.061692326	0.034869576	0.037551851	0.0321873	0.037551851	0.050963226	0.061692326	0.050963226	0.059010051	0.029505025
Myristoyl Carnitine		0.030490416	0.038952926	0.04585084	0.044296263	0.033713116	0.039542363	0.043139096	0.068675237	0.036526717	0.073692965	0.027017247	0.047076468
Cotinine	ND	0.024645794	0.035208277	1.922371938	0.056333244	1.707601447	0.014083311	0.028166622	1.545643372	0.007041655	0.014083311	0.014083311	0.024645794
Arachidyl Carnitine	RT shift	0.02094588	0.043063963	0.017932679	0.020750029	0.017696207	0.032264605	0.022376316	0.035744946	0.028254741	0.03649063	0.012701287	0.023657325
Dodecanoyl Carnitine		0.010253494	0.01032574	0.017044605	0.018196927	0.014198118	0.015124672	0.014983792	0.02619635	0.011965721	0.02198261	0.011745371	0.019251717
4-Pyridoxic Acid		0.010160983	0.003386994	0.003386994	0.003386994	0.003386994	0.003386994	0.020321965	0.003386994		0.013547977	0.010160983	0.003386994
5-Deoxy-5Methylthio Adenosine	<LLOQ but quantify since the resp. is good	0.003403755	0.002959242	0.004455559	0.002130738	0.002817332	0.004215564	0.002750551	0.003355756	0.006857595	0.006396388	0.004904245	0.003652097
Kynurenic Acid	mostly ND	0.003279684		0.009839053			0.003279684	0.019678106	0.006559369		0.009839053	0.013118737	0.003279684
Stearoyl Carnitine		0.001293376	0.00529331	0.001311075	0.000841375	0.001036062	0.001813449	0.001556135	0.00279233	0.002396149	0.003263391	0.000352615	0.001611955
Orotic acid	minor concentrations		0.278174627	0.484818636				0.290096397			0.413288017		0.544427484
Homogentisic acid	ND												
D-Glucuronic acid	ND												
Gamma-Glutamylcysteine			0.441329938					0.10413403		0.10413403		0.10413403	
cGMP	ND												
Spermidine													
Adenine	ND												
Pyridoxine	ND												
5-Hydroxyindole-3-acetic acid	ND												
L-5-Hydroxytryptophan	ND												
Nicotinic Acid	ND												

ULOQ = Upper limit of quantification
LLOQ=Lower limit of quantification
ND=Not detected
RT=Retention time

TABLE S2. Heart

Units: µmoles		AOX						WT					
Metabolite name	**Comments**	**1_MS 213**	**2_MS 214**	**3_MS 216**	**4_MS 223**	**5_MS 240**	**6_MS 250**	**7_MS 215**	**8_MS 224**	**9_MS 230**	**10_MS 241**	**11_MS 267**	**12_MS 234**
Glutamine		75825.93431	57284.67332	65654.56736	42218.23423	59416.85686	79586.1489	66430.15259	64585.53283	61683.40254	52893.54611	90361.74882	60735.42981
Taurine		46296.51904	43392.96665	41854.48966	35973.24357	42462.36753	54187.79352	46113.82002	47806.2438	38373.14472	39624.51008	44551.98417	44331.82618
Alanine		24567.58807	27069.97198	20811.47156	20861.28577	22502.20715	24372.24544	20971.55131	25271.3872	22200.05666	24447.63551	21287.83559	23473.76889
Cysteine	>ULOQ	5874.963696	5875.961221	6002.108476	5991.638436	5728.41675	5988.856679	5655.458247	5859.386971	5532.170366	5287.459678	6732.340556	6009.395924
Hydroxyproline		4620.287322	4989.901781	3788.642962	4050.210353	4202.529828	4463.087209	3811.11403	4625.109015	4337.73767	4678.069485	3979.726534	4195.477695
Creatine		4370.923915	4328.274441	4286.581438	3435.448146	4292.294713	4975.578898	4375.430959	4723.199993	3860.274024	4410.217229	4509.05292	4529.253734
Acetoacetic acid		1651.305502	2206.819748	1678.984582	1697.745423	1588.034224	2128.072365	1758.054386	1884.055643	1571.903189	1567.134865	2525.569262	1874.24549
Hypoxanthine	dil. also >ULOQ	1284.848284	1592.444839	1535.00215	966.9480583	1186.214157	1639.452601	1471.149747	1513.469175	1185.541465	1084.950789	1360.703862	1219.408492
Succinate		1153.082665	1215.158566	995.6500437	731.5437872	847.0907209	671.7676728	844.6941732	861.5760661	1065.436848	1057.552541	816.2904974	1073.775596
Adenosine		976.1713865	1113.865294	1555.140532	1078.772077	1199.811435	1250.61004	1217.40679	1602.78664	966.2347846	489.3879181	343.2852593	629.4300087
Myoinositol		788.9179869	706.5085342	685.4700771	669.810086	653.0190621	612.9110224	522.5719443	587.2085699	437.8337995	530.1094889	668.8234279	848.3347072
Glycine		672.8043603	741.9611236	459.8442068	530.1305411	404.0357992	571.9074793	410.9461789	455.7965087	618.2739296	621.204782	570.5963672	374.8279202
Inosine		647.6025473	727.9636384	798.91097	493.5438191	640.8516716	793.2112328	651.6135248	770.2221771	550.9470765	490.5652468	723.2428822	607.292951
Lysine		547.4171703	543.4053578	396.6758383	413.9880783	551.0362462	566.9165568	406.508471	397.5211876	381.8066708	675.6512748	452.4725382	455.4991779
Carnitine		537.2615547	466.3481948	540.9070449	448.359038	369.0248795	357.2537643	355.9039319	420.6286521	417.1753904	508.4479163	389.6827597	404.8321695
Aspartate		531.1613103	418.9412571	387.9103837	350.4216773	333.7507094	503.6340805	260.2133416	505.0755236	313.865505	445.9525872	234.0940005	257.5569479
L-Glutamic Acid		525.9784757	421.0478929	566.9013904	399.128065	428.3346862	584.8432691	585.3479438	522.3825109	303.0526878	440.0560391	454.76117	564.5171506
Serine		525.3274712	562.2104214	452.1858052	392.6647376	385.5435312	344.591902	402.7489325	576.1365263	413.6453522	531.053594	265.1944347	445.5565021
Threonine		418.250486	473.260337	326.2805701	287.3948106	311.7698251	358.4567328	336.5689413	342.1699579	379.2305804	376.8636515	258.9507322	421.3926087
AMP		351.8229931	339.3245464	283.3118147	416.4977658	406.9842105	580.2210808	266.2025854	348.7560515	365.5309346	442.0819443	620.4910865	396.0622248
Asparagine		337.6734824	339.7248511	244.0262888	181.6746739	158.6636816	219.4971936	239.6091699	209.5636528	198.0195163	271.3284314	319.6446134	203.0405617
Citrulline		314.3037983	308.3282108	282.5626991	281.8029237	275.632019	280.3683195	225.4760414	257.0914733	211.2307746	273.6011592	318.5968109	278.9231634
Acetylcarnitine		288.2094793	358.3018654	258.6582854	251.2419084	273.5726618	232.1987315	241.2679473	345.9307876	276.2099146	231.5016748	172.9543744	247.0849339
Arginine		254.1208818	276.3308118	211.0840169	212.7028882	289.3218783	314.6105552	195.8941812	230.8830529	217.4539561	345.2914816	328.4077101	259.4007482
Niacinamide		246.2204628	287.4428794	271.0767464	189.8526295	224.3070047	328.837507	255.0458913	249.6738251	203.3582325	229.1685341	310.3743632	281.5587525
Proline		229.3821493	165.0077959	132.9471912	114.2604388	107.6201218	114.1632332	133.4597837	121.1851522	172.7603734	191.7037723	142.9034907	113.8181641
Histidine		228.6186102	211.624947	173.3164373	152.8977093	110.9988489	196.6107165	199.5983774	161.4222085	201.7843976	222.5904721	182.424475	158.3732151
Leucine		208.7907305	174.0459463	164.1421405	134.5559107	104.072323	126.8752104	106.3182242	116.0024909	153.1714276	219.5434176	134.1475736	144.5154762
IMP		205.5363951	155.1607288	130.2625462	138.6116406	136.9816887	195.9089909	227.968808	161.7468032	126.8214773	188.7543039	336.2072309	227.4279846
Tyrosine		193.5359883	138.1371488	134.9390833	131.6580538	133.7546475	132.6862517	109.9026067	106.9781885	129.0214927	160.4715628	201.7823894	122.1141558
Valine		186.3127898	175.3715584	114.7767799	118.056009	123.5250625	175.7923974	119.8185867	128.9276566	139.1704552	162.7437407	99.61868561	136.5367031
Glutathione		158.9653822	2715.967117	387.7132145	571.5241814	108.5039468	365.9580012	1349.571445	1497.926898	681.7792815	227.3007595	80.95773701	240.8464854
Creatinine		156.8824003	168.3715943	143.0888307	120.16402	91.45427843	102.1151344	86.07767628	113.5419769	108.5603776	209.5308098	102.2783343	110.2349311
L-Methionine		152.380112	134.6859656	112.5379172	89.40095399	94.30497158	82.32035874	107.8630131	101.360193	127.209247	128.085061	104.7158646	100.0594709
Glyceraldehyde		142.8482612	101.3387919	107.9989665	87.69291943	66.79635803	97.22950117	91.51049953	87.64133981	116.7051785	141.8151539	141.6523579	104.302175
Choline		125.6293493	165.4958581	179.1527368	155.5390572	129.8904241	133.3457359	135.8166233	170.5180305	99.14815389	114.7971075	152.2248879	83.74753966
D-Ribose 5-phosphate	bad chromatography and unreliable values	123.2469783	145.7364685	87.06832714	125.3497354	129.8990514	156.7489081	90.43009158	125.2473092	127.3225729	141.9741904	223.2039785	108.8415612
Betaine		111.8521951	74.66044951	21.92286798	108.3474805	64.06565435	65.72004356	30.05506394	78.11141401	138.6307836	72.78512909	77.4965453	79.35153073
Isoleucine		92.16972762	91.47762607	60.30699731	68.62361377	70.04896272	89.33099512	55.58648071	69.21592482	74.92659025	90.05289194	52.63272902	79.10573152
Phenylalanine		91.51982216	77.37004116	69.75215906	63.00787092	61.63389465	72.65762893	62.23346705	64.30196179	76.53160128	78.55547738	108.1306518	70.49306138
Xanthine		72.63953891	108.5617392	81.45167571	71.09049147	80.3202614	99.76791289	116.8543324	83.47108549	132.2423663	71.92722585	96.02055158	97.47360173
Phosphoethanolamine		63.9958708	66.46537902	38.6998217	41.89348862	47.49023162	49.58159104	40.18990649	56.04340275	46.00718134	46.38119737	33.81404769	44.43980488
Pantothenic Acid		63.93577945	74.93029732	53.39332171	42.48493747	51.71753569	55.4821474	52.72159815	55.87393662	65.78957688	64.65832299	44.57367827	51.49108118
Xanthosine		61.51707796	78.77594198	74.17473788	53.04753715	61.67378268	75.89918819	47.38246516	92.33993572	57.04771972	42.16926148	38.69674604	44.8892669
Uracil		51.33324184	64.59452486	48.58249565	45.24233942	49.61526378	46.27389	45.25069631	49.65084976	48.76955724	48.41491503	29.22488653	31.88758095
deoxycytidine		47.33793415	39.23790384	33.27995156	55.66781897	39.71664227	59.98681222	42.23616876	38.92275826	35.2739715	31.90977952	68.98414605	55.52650445
Ornithine		46.80701717	48.96169407	21.6722805	25.22964478	17.97105204	28.59043381	17.69740503	23.98729671	33.05900042	37.72958705	32.04570852	27.44515299
Adenine		38.58291745	44.8486803	49.66780926	31.8882877	30.79316675	28.55609931	32.38316943	42.46016436	42.65490353	27.63620689	19.41951741	30.04611568

Units: µmoles		AOX						WT					
Metabolite name	**Comments**	**1_MS 213**	**2_MS 214**	**3_MS 216**	**4_MS 223**	**5_MS 240**	**6_MS 250**	**7_MS 215**	**8_MS 224**	**9_MS 230**	**10_MS 241**	**11_MS 267**	**12_MS 234**
Allantoin		38.12664412	46.75217041	37.93806751	48.4581081	38.5387509	27.89105724	30.30822728	59.09411134	41.60791662	38.11530677	11.86977365	39.00126769
S-5-Adenosyl-L-Methionine		35.94597564	25.75399971	28.67269638	34.34541638	29.69579041	86.80537191	45.6922704	25.09975791	19.93774698	16.96891336	142.5954194	28.7080122
Aminodipic Acid		34.31323466	36.42749389	33.88838889	27.30006522	29.17786276	28.429138	26.78464573	30.28387831	22.09136441	28.30711561	29.25665766	39.81309552
Guanosine		32.9196611	52.32145735	41.83933844	30.05984616	31.5495982	39.1659889	26.42081439	51.29407991	27.27869974	23.9225198	19.32496743	20.60766711
GABA		31.56182841	29.41138949	17.27906876	17.0726093	10.16193228	10.21986365	23.09638893	18.00414332	15.36877733	18.13727117	7.497690837	42.70684942
Tryptophan		31.2465125	33.89274668	25.00215567	25.71833525	27.23119815	27.87796224	22.65089938	23.22800493	24.06615529	30.54476284	32.65970266	26.7084706
Homoserine		20.41416318	20.28126688	16.10466736	17.31495063	16.29078467	20.22846247	11.42309315	19.13139101	23.93013477	18.13565819	24.46697958	19.08030509
3-Hydroxyanthranilic acid		18.89695971	16.11150366	17.15317842	17.58572076	14.7142991	12.10519004	0.33328893	14.68440154	15.98859146	10.67257835	15.4997785	9.207233278
Homocysteine		13.93165052	15.02917605	13.47241982	10.25284629	11.27608316	11.96653618	14.82981796	12.87361092	12.84468517	12.66511596	9.547654911	11.9450944
Taurocholic Acid		11.71288292	11.78228361	10.22875729	8.447428728	8.371193848	7.215434081	8.204911328	9.777315891	9.73395249	9.271405537	5.91820182	7.907359468
Carnosine		11.2949688	11.97423429	8.004375529	11.13814983	8.745200488	11.21320028	11.72391075	9.890645245	6.208676375	11.63432734	14.63733234	12.34444112
Trimethylamine-N-Oxide		8.050259435	4.663519395	6.524549813	3.419281023	2.894165353	6.790246119	4.085958231	6.277519148	1.879778649	4.802850967	3.346600653	3.229320966
S-Adenosyl-L-Homocysteine		5.664102371	5.238406953	6.315154557	6.463084279	5.484214017	7.516282569	5.433241615	5.981380554	3.922486122	5.47399694	7.634400377	5.493559496
Guanidinoacetic Acid		5.345862043	5.931148341	3.777612564	4.538378818	4.497647129	5.472241509	3.776818058	3.823535028	4.623073189	8.37256023	7.489598909	3.935984151
Asymmetric dimethylarginine		5.3197634	7.591315009	5.526519039	5.868228663	4.277182524	6.465522732	6.201534335	6.442856597	5.090679011	5.360096239	5.348594479	4.477803891
Nicotinic Acid		5.294177545	6.093970913	7.820448184	7.41316887	6.548569613	6.736788895	6.813941163	7.765418611	6.053908174	3.115419669	2.911729619	4.188849102
Hexanoylcarnitine		4.983833815	6.550134426	5.344454221	4.441240645	4.824132201	4.451526998	3.708302096	5.661991553	4.612855291	5.493343203	2.239171641	6.055552211
cGMP		4.611698825	4.221979063	6.300202954	4.14597212	6.156867874	0.180529967	4.863671725	4.96916505	4.698594707	4.290618903	13.08153166	5.685678732
DimethylGlycine		3.688237054	4.829418866	2.559387465	2.798692749	1.542249769	2.056593707	2.914675803	3.411874943	2.850728715	2.006783557	1.985548071	2.909321814
Propionylcarnitine		3.230358073	2.172627176	2.438066434	2.845448306	1.775410576	2.537948805	1.902533594	2.109551088	1.75873496	2.181164863	2.63620359	2.754817476
Sorbitol	bad chromatography and unreliable values	2.114916675	2.740163817	4.784832978	1.828546538	8.040292787	47.8859563		5.028468927	5.488363705	15.7307441	13.67602985	11.95256515
Cytidine		1.961647852	1.974298544	2.339459734	1.713531064	1.594318701	1.599572819	1.828356494	1.885590671	1.521143632	1.772703653	1.349160542	1.412873097
Symmetric dimethylarginine		1.743544142	2.248241375	1.477899492	1.5448244	1.152077632	2.166931599	1.857396232	1.510717847	1.114842601	1.516238692	1.112542249	1.436769198
D-Glucuronic acid		1.329703561			2.831499187					1.827064327	1.718747932		
1-methylhistamine		1.036643271	0.941880318	0.665174476	0.930233198	0.879332804	0.803205243	0.771782799	0.953031816	0.743334088	1.230976713	0.61377846	0.784222915
Glycocholic Acid		0.932446936	0.705064728	0.611140486	0.665690897	0.438788369	0.704611695	0.57722969	0.501693227	0.561666701	0.53044745	0.836164262	0.715271277
Sucrose	bad chromatography and unreliable values	0.904602559	0.82310569	0.856360472	0.740920166	0.723540692	0.64470783	0.691989425	0.878379306	0.648350452	0.707357302	0.692659957	0.927944335
NAD		0.866558828	1.432573299	1.450367153	3.198132531	1.926824204	4.049110068	1.538832296	0.226148123	1.079599621	1.727516234	4.709788589	2.320594914
Cytosine		0.808198542	0.845104879	0.785362396	0.956996408	0.829694669	0.80462516	0.591227244	1.043874262	0.890498	0.789549954	0.530033075	0.77709895
2-deoxyuridine		0.712087139	0.827864162	1.162826472	0.729512138	0.574046349	0.882286703	0.743212917	0.850997819	0.457644092	1.10266809	0.771022238	0.77822602
3-OH-DL-KYNURENINE		0.636491357	0.684911626	0.47797723	0.667203642	0.640032954	0.693654944	0.521140441	0.808148129	0.569920404	0.640171298	0.549473216	0.528527991
L-5-Hydroxytryptophan		0.631564762	0.865158366	1.067510375	1.09638561	1.173602212	0.743403475	1.012689686	1.33454291	1.218027817	0.865580931	1.179067379	0.890850282
Taurochenodeoxycholic Acid		0.62795121	0.718635957	0.780065157	0.57695268	0.479537667	1.392792554	0.706392337	0.652997237	0.657504777	0.375019863	0.451374856	0.340933922
2-Aminoisobutyric acid		0.579073069	0.656916468	0.494672538	0.618235397	0.519457298	0.643982673	0.514945509	0.625815203	0.534737224	0.449975749	0.738670083	0.560424342
Hippuric acid		0.576931831	0.979038982	0.663461218	0.64351687	0.541821468	0.727726341	0.772601125	1.837684736	0.834269328	0.501690391	0.242967871	0.678419479
Octanoylcarnitine		0.465264998	0.621835639	0.457342562	0.69726068	0.717897869	0.472323953	0.370497989	0.725107933	0.460170462	0.570091557	0.18864895	0.776506623
Cystathionine		0.336429346	0.201382977	0.094228136	0.273191797	0.189768487	0.299240642	0.102939004	0.016584152	0.116898728	0.293377558	0.140909453	0.270148577
Decanoylcarnitine		0.301542026	0.356788019	0.361232872	0.63952792	0.439135818	0.31682367	0.229047642	0.370810942	0.265452174	0.449736598	0.088916743	0.474124291
Normetanephrine		0.274359749	0.401651566	0.322919596	0.263049436	0.179542754	0.264505554	0.210527593	0.231759828	0.190141939	0.339817339	0.17402305	0.11120679
Gamma-Glutamylcysteine		0.251979559	0.209235019	0.252896931	0.247541466	0.289517398	0.313542606	0.170209552	0.218185587	0.282996624	0.218755845	0.197086049	0.228822135
L-Kynurenine		0.232345667	0.20195421	0.157767416	0.186281753	0.107055396	0.316637266	0.111852479	0.202579917	0.486412287	0.23854314	0.230230183	0.251831954
cAMP		0.206168911	0.281480293	0.172837454	0.186761675	0.209805413	0.212537499	0.200855474	0.241252672	0.216871154	0.1862341	0.236711756	0.225067414
Orotic acid	minor conc	0.132967472	0.097281641	0.077332546	0.056906581		0.066722171	0.054959358	0.087942921	0.103202787	0.077014632	0.074471322	0.136305567
Isobutyrylcarnitine		0.123438297	0.127890874	0.140578035	0.113352943	0.099244176	0.082050793	0.090365846	0.121372945	0.111636287	0.126254686	0.061692326	0.106405851
Kynurenic Acid	minor peaks at shifted RT	0.065036139	0.040832069	0.032698452	0.059690254	0.027910113	0.060182206	0.036437292	0.033485576	0.036306105	0.036240511	0.047948984	0.050802309

Units: µmoles		AOX						WT					
Metabolite name	**Comments**	**1_MS 213**	**2_MS 214**	**3_MS 216**	**4_MS 223**	**5_MS 240**	**6_MS 250**	**7_MS 215**	**8_MS 224**	**9_MS 230**	**10_MS 241**	**11_MS 267**	**12_MS 234**
Stearoyl Carnitine		0.063673269	0.084825155	0.144726483	0.289728609	0.176584879	0.154896217	0.138575318	0.125460568	0.121848209	0.17509061	0.005367763	0.106934534
Palmitoyl Carnitine		0.031191366	0.040553433	0.04724506	0.267975597	0.115449973	0.118198043	0.048161084	0.066171031	0.044931714	0.130820532	0.002903328	0.034544942
Isovalerylcarnitine		0.021318903	0.016033434	0.019093443	0.016438063	0.015173597	0.016134591	0.010191599	0.016109302	0.014516074	0.020029148	0.012973425	0.015021861
Dodecanoyl Carnitine		0.019903735	0.027345059	0.025105438	0.069590828	0.054148275	0.050897211	0.02808558	0.036520284	0.027345059	0.041938724	0.007152341	0.040259008
Myristoyl Carnitine		0.018868658	0.025748205	0.02771856	0.109471615	0.069012536	0.079298459	0.03279473	0.038972963	0.028970905	0.05914406	0.003172606	0.030089666
5-Deoxy-5Methylthio Adenosine	>ULOQ	0.011519759	0.013836232	0.018990906	0.018448309	0.0172379	0.025335121	0.019408289	0.017843104	0.013564933	0.01291799	0.024709047	0.018197879
Pyridoxine		0.009644304	0.007407412	0.008140819	0.009130919	0.008727545	0.009130919	0.008837556	0.009717644	0.008654204	0.008067478	0.009937666	0.00825083
Chenodeoxycholic Acid		0.008408008	0.027247005	14.30153229	4.223522773	10.78415578	0.126926156	20.54828739	3.107470294	1.505618265	0.116100055	47.57584608	5.283105676
4-Pyridoxic Acid		0.004132133	0.002269286	0.001016098	0.001625757	0.001219318	0.001998327	0.002574116	0.002167676	0.002337026	0.002946685	0.001117708	0.001862847
Arachidyl Carnitine		0.003458078	0.004819526	0.007365434	0.012879299	0.009189775	0.006357963	0.011912671	0.005064587	0.004520008	0.006671096	0.000694339	0.005881456
5-Hydroxyindole-3-acetic acid						0.031282607					0.088396081		
Neopterin	ND												
Folic Acid	ND												
Homogentisic acid	ND												
Cholic Acid	ND												
UDP-Glucose	ND												

ULOQ = Upper limit of quantification
LLOQ=Lower limit of quantification
ND=Not detected
RT=Retention time